**Key Points:**
- When continents collide, the lower crust is dry and strong and subject to high mechanical stress
- Introduction of fluids to the lower crust is often associated with earthquakes
- Fluid-induced metamorphism may cause a transition from brittle to ductile deformation of the lower crust

**Correspondence to:**
B. Jamtveit,
bjorn.jamtveit@geo.uio.no

# The Effects of Earthquakes and Fluids on the Metamorphism of the Lower Continental Crust

Bjørn Jamtveit[1], Arianne Petley-Ragan[1], Sarah Incel[1], Kristina G. Dunkel[1], Claire Aupart[1], Håkon Austrheim[1], Fernando Corfu[2], Luca Menegon[1,3], and François Renard[1,4]

[1]The Njord Centre, Department of Geoscience, University of Oslo, Norway, [2]Departments of Geoscience, University of Oslo, Norway, [3]School of Geography, Earth and Environmental Sciences, University of Plymouth, Plymouth, UK, [4]Université Grenoble Alpes, Université Savoie Mont Blanc, CNRS, IRD, IFSTTAR, ISTerre, Grenoble, France

**Abstract** Rock rheology and density have first-order effects on the lithosphere's response to plate tectonic forces at plate boundaries. Changes in these rock properties are controlled by metamorphic transformation processes that are critically dependent on the presence of fluids. At the onset of a continental collision, the lower crust is in most cases dry and strong. However, if exposed to internally produced or externally supplied fluids, the thickened crust will react and be converted into a mechanically weaker lithology by fluid-driven metamorphic reactions. Fluid introduction is often associated with deep crustal earthquakes. Microstructural evidence, suggest that in strong highly stressed rocks, seismic slip may be initiated by brittle deformation and that wall-rock damage caused by dynamic ruptures plays a very important role in allowing fluids to enter into contact with dry and highly reactive lower crustal rocks. The resulting metamorphism produces weaker rocks which subsequently deform by viscous creep. Volumes of weak rocks contained in a highly stressed environment of strong rocks may experience significant excursions toward higher pressure without any associated burial. Slow and highly localized creep processes in a velocity strengthening regime may produce mylonitic shear zones along faults initially characterized by earthquake-generated frictional melting and wall rock damage. However, stress pulses from earthquakes in the shallower brittle regime may kick start new episodes of seismic slip at velocity weakening conditions. These processes indicate that the evolution of the lower crust during continental collisions is controlled by the transient interplay between brittle deformation, fluid-rock interactions, and creep flow.

**Plain Language Summary** When continents collide, a mountain range form along the collision zone in an area referred to as an orogenic belt. The evolution of orogenic belts depends on the physical properties of the different layers in the Earth's crust and upper mantle. During a continent-continent collision, the mechanical strength and density of these layers change. We discuss transformation processes in the lower part of the continental crust during the formation of an orogenic belt. We emphasize the critical role of fluids and show that introduction of fluids to initially dry lower crust is often associated with earthquakes. Earthquakes cause fracturing and fragmentation and allow fluids to migrate into highly reactive dry rocks. This results in the formation of weaker rocks, which subsequently deform slowly along zones where earthquakes initially occurred. Earthquakes in the upper crust may subsequently send stress pulses to the lower crust to trigger new generations of earthquakes.

## 1. Introduction

The continental lithosphere's response to plate tectonic and buoyancy forces operating at plate boundaries is strongly affected by the rheology and density of the various lithospheric units (Burov, 2011; Butler et al., 2015; Chen & Molnar, 1983; Clark & Royden, 2000; Copley et al., 2011; Nakao et al., 2016; Pristley et al., 2008; von Blanckenburg & Davies, 1995). These material properties determine whether mechanical stress is dissipated through earthquake activity or by slower creep process, as well as where and when mountain belts and sedimentary basins form and how they evolve. Rock rheology and density evolve with time during a variety of metamorphic transformation processes that are critically affected by the presence of locally produced or externally derived fluids. Hence, fluids play a central role in the geodynamics of an orogeny.

For a long time, fluid migration during metamorphism was considered as a Darcy flow process with lithostatically pressurized fluid migrating upward through rocks characterized by a time-independent permeability (Walther & Orville, 1982). As pointed out by Connolly (1997), such a model is a mechanical impossibility as it would require a perfect balance between the rates of chemical, mechanical, and hydrodynamic processes. Over the last couple of decades, a more dynamic description of fluid migration has emerged, where metamorphic fluid flow patterns may display considerable spatial and temporal complexity, and where fluid flow is not always upward directed (Connolly, 1997, 2010; Connolly, 2010; Connolly & Podladchikov, 1998; Jamtveit et al., 2000; Jamtveit & Yardley, 1997; Plümper et al., 2017). Yet our understanding of how fluid migration and fluid-controlled metamorphism are coupled to plate tectonic stress and how metamorphism-induced changes in rock properties provide feedback on the geodynamic processes at plate boundaries are still poorly understood.

For upper crustal conditions, observations from deep continental boreholes at several locations worldwide indicate that the brittle crust is in a state close to failure equilibrium, that hydrostatic fluid pressure may persists to depths reaching 12 km and that bulk permeabilities are high (Zoback & Townend, 2001). In an upper crust at a state of high differential stress, inflation of fluid pressure by natural (Miller et al., 2004) or man-made processes (Ellsworth, 2005) may trigger earthquakes. On the other hand, earthquake-induced breaching of overpressured fluid reservoirs may cause highly focused fluid flow, occasionally leading to significant mass transfer (metasomatism) and hydrothermal mineralization (Sibson, 1996).

For the lower crust, the situation prior to an orogeny is very different. Near a steady state geothermal gradient, lower crustal granulites and amphibolites will remain dry (no fluid phase present), and impermeable (Jamtveit et al., 2016; Yardley, 1995; Yardley & Valley, 1997). As discussed below, a rheology controlled by dry plagioclase is sufficiently strong to develop differential stress levels approaching 1 GPa even at strain rates of $10^{-14}$ s$^{-1}$ for realistic lower crustal temperatures (Tullis & Yund, 1992; Rybacki & Dresen, 2004). Irrespective of changes in pressure and temperature conditions, significant progress of metamorphic reactions in lower crustal rocks will depend on local fluid production by devolatilization reactions or the introduction of externally derived fluids. Hence, in the absence of fluid supply, the lower crust will remain mechanically strong throughout an orogenic event. This is in stark contrast to some of the established models for lithospheric strength, such as the jelly-sandwich model (Chen & Molnar, 1983), where the lower crust is assumed to be mechanically weak and to deform by ductile mechanisms operating at relatively low differential stress conditions. Such models were partly based on the low frequency of earthquakes observed in the lower crust, and the common observations of ductile shear zones in lower crustal lithologies that had experienced an orogenic event.

In this article, we review recent developments in the study of the lower continental crust, and argue that the scarcity of earthquakes in this part of the lithosphere arises because the lower crust is strong, not weak. During an orogeny, the lower continental crust may locally become weaker and develop into shear zones, but mainly in situations where fluids are introduced either by fluid release during prograde metamorphic reactions or by influx of fluids along highly localized pathways. These pathways may in many cases be generated by earthquakes that penetrate the deep crust and connect its dry rocks to some external fluid reservoir. We also demonstrate that the wall rock damage caused by dynamic earthquake ruptures on subsecond timescales plays a very important role during the incipient stages of lower crustal metamorphism that may subsequently proceed on timescales relevant to the evolution of the entire orogeny. Finally, we emphasize that when highly stressed lower crust is locally weakened, the weak portions may experience a significant increase in pressure and develop mineral assemblages that until recently have been taken to indicate extremely deep burial of continental crust.

## 2. The India-Asia Collision

Over the last couple of decades, seismic imaging, gravity anomaly studies, Global Positioning System (GPS) data, along with thermodynamic and geodynamic modeling have put tight constraints on the density and rheology of the Indian crust prior to and during subduction beneath the Tibet plateau. Figures 1a and 1b show the distribution of earthquakes across the India-Asia collision (from Craig et al., 2012). Although earthquakes do occur at all crustal levels (Shi et al., 2018; Sloan et al., 2011), there is a bimodal distribution of the frequency of seismic activity below the Tibetan plateau, with numerous earthquakes in the shallow
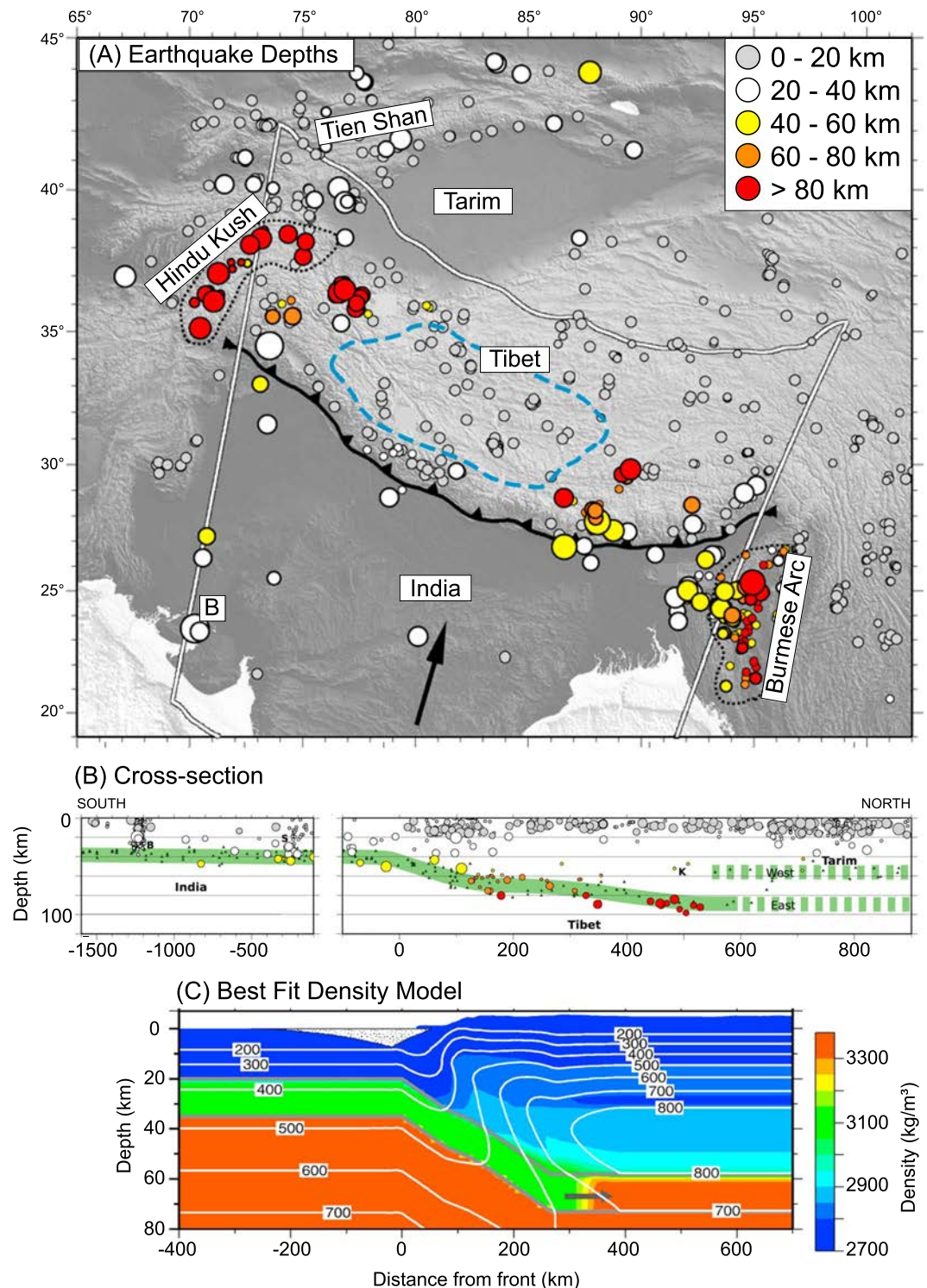
**Figure 1.** (a) Earthquake depth distribution during the subduction of India under Tibet (from Craig et al., 2012). The Bhuj 2001 earthquake (marked by B) occurred in a strong Indian crust. Black arrow indicates the direction of convergence. Dashed blue line denotes area without deep crustal earthquakes. (b) Earthquake distributions in cross sections from the eastern and western regions of the orogen, illustrating a bimodal distribution of earthquakes frequency with depth under Tibet (from Craig et al., 2012). (c) Thermal field and best fit density model of the India/Tibet crust. Arrow marks the metamorphic transition toward a dense eclogite facies mineralogy in the lower part of the Indian crust. The transition is interpreted to have developed within a time interval of less than 6 My (from Hetényi et al., 2007).

(<20 km) "seismogenic" regime, but also relatively frequent deep earthquakes distributed along the Moho of the subducted Indian plate (Monsalve et al., 2006). Deep earthquakes are, however, focused on the eastern and western parts of the orogen (Figure 1a) where the subduction angle may be steeper than those in the central parts (Shi et al., 2016). The compressive stress generated during plate collision is transferred through the Indian lithosphere, causing large intraplate earthquakes such as the 2001 $M_W$ 7.6 Bhuj event that occurred nearly 1,000 km south of the Main Central Thrust. This put constraints on the strength of the Indian lithosphere, and Copley, Avouac, Hollingsworth, and Leprince (2011) calculated an effective viscosity $>10^{24}$ Pa s for the lower crust in order to prevent stress release by ductile flow. This is similar to the lower crustal viscosity necessary to explain the pattern of strain within the Tibetan Plateau reported by Copley et al. (2011). The latter authors concluded that this would imply a rheology controlled by dry and metastable granulites, as these viscosities are consistent with the rheological properties measured for dry plagioclase aggregates at relevant temperatures (Rybacki & Dresen, 2004).

The low frequency of earthquakes at 20- to 60-km depth under the Tibetan Plateau (Sloan et al., 2011) may thus not imply that this intermediate region is weak and undergoes ductile flow. In contrast, it is easier explained by a strong crust where frictional sliding only occurs at very high differential stress levels. The relatively higher abundance of earthquakes near the Moho and the lower part of the subducted Indian crust in the eastern and western parts of the orogen then requires local weakening mechanisms. One possible mechanism is the introduction of fluids by dehydration of the subducted crust and/or upper mantle. Fluid introduction would not only weaken the crust by reducing the effective confining pressure but would also drive metamorphic reactions. Based on a combination of gravity anomaly data and petrological modeling, Hetényi et al. (2007) proposed that eclogitization of metastable lower Indian crust occurs when amphibole present in the granulites breaks down to liberate aqueous fluids during subduction and heating to ca. 700 °C. Figure 1c shows the thermal field and density distribution in a cross section modeled by Hetényi et al. (2007). They concluded that when eclogitization starts, the lower Indian crust is converted to a high-density state within a timescale of less than 6 Myr, and at least 100 °C above the equilibrium temperature.

An alternative fluid source is dehydration of the mantle. The pressure and temperature path during subduction of the Indian lithosphere (cf. Figure 1c) is such that any serpentine present in the Indian mantle will lead to fluid production near Moho depths from a series of devolatilization reactions. A low effective mantle viscosity (~$10^{19}$ Pa s) of the Indian lithospheric mantle was inferred from postseismic deformation following the Bhuj earthquake (Chandrasekhar et al., 2009). This would be consistent with a somewhat hydrated mantle lithology. Interestingly, Schulte-Pelkum et al. (2019) recently concluded that the deep earthquakes beneath southern Tibet nucleate below Moho. Dehydration of a partially hydrated mantle would then be a plausible trigger mechanism.

The results from the India-Asia collision emphasize that when the continental lithosphere enters a convergent plate margin, its lower crust is likely characterized by relatively low density and high mechanical strength. During the orogeny it may be converted into a weaker state through the introduction of internally produced or externally derived fluids. This weakening of the lower crust may subsequently play a key role during gravity driven extension and orogenic collapse of thickened crust (Bischoff & Flesch, 2018).

Insights into the mechanisms by which lower crust is weakened by interactions with fluids do, however, require studies of lower crustal lithologies from former collision zones that have subsequently been exposed at the surface to allow sampling and direct studies of the various metamorphic transformation processes that have been operating at depth. In the following, we will describe observations from lower crustal volumes that experienced both earthquakes and associated fluid-induced metamorphism during the Caledonian orogeny: the Lindås Nappe of the Bergen Arcs in Western Norway, and the Proterozoic basement of the westernmost Lofoten Islands in Northern Norway.

## 3. The Bergen Arcs

The Lindås Nappe in the Bergen Arcs is composed of granulite facies remnants of Proterozoic lower crust belonging to the former Jotun-Lindås microcontinent (Figure 2). Before the Caledonian plate convergence between Baltica and Laurentia, the Jotun-Lindås microcontinent was separated from the margin of Baltica by a hyperextended domain with transitional thinned crust (<10 km), exhumed metaperidotites, and extensional allochthons of continental crust (Jakob et al., 2017). The profile in Figure 2 illustrates the
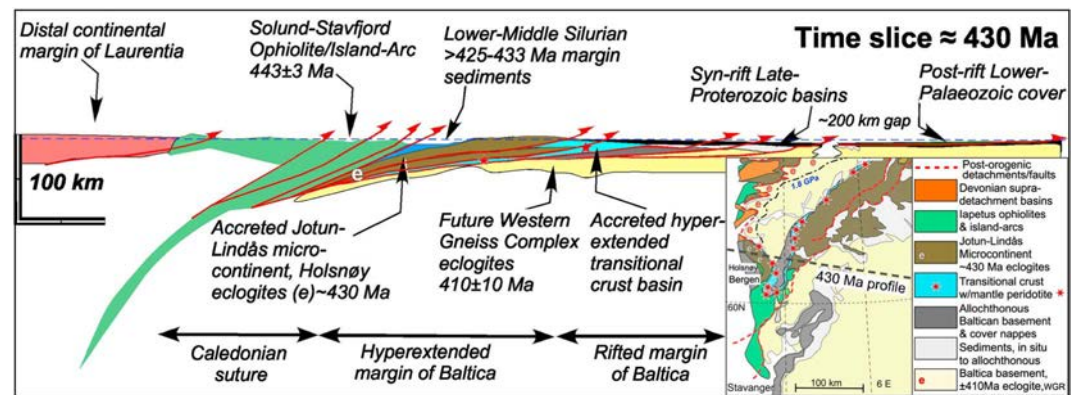
**Figure 2.** E-W profile across the Bergen Arcs at 430 Ma, prior to the final continental Scandian collision. The leading edge of the Jotun-Lindås microcontinent is buried beneath the accreted outboard ophiolite/island arc terrains in the west, while it is thrust upon the hyperextended margin of Baltica in the east. The eclogitized and amphibolitised shear zones in the Lindås nappe formed at this stage, before the main continent-continent collision between Baltica and Laurentia (from Jamtveit, Moulas, et al., 2018).

tectonic setting in the Middle Silurian, at ~430 Ma. At this initial stage of the Scandian collision, ophiolites and Laurentian island-arc complexes were emplaced onto the Jotun-Lindås microcontinent and its fossiliferous Middle Silurian cover. These events caused fluid-induced metamorphism transforming the 930-Ma-old anhydrous granulite facies mineralogy (Bingen & Austrheim, 2001) to eclogites and amphibolites in shear zones, breccias, and along fractures located near the leading edge of this microcontinent (Austrheim, 1987, 2013; Putnis et al., 2017). The eclogites and amphibolites are now exposed on Holsnøy Island (Figures 3a and 3b). The hyperextended Baltic margin closed during the collision, which continued into the Lower Devonian and resulted in large-scale nappe translation (>600 km) onto Baltica and formation of a Himalayan-type mountain belt. The regional ultrahigh pressure (UHP) metamorphism and metamorphic zonation in the Western Gneiss Complex at 410 ± 10 Ma (see inset map in Figure 2) formed during the terminal stages of the collision (Hacker et al., 2010).

### 3.1. Paleoearthquakes

On the island of Holsnøy, pseudotachylytes, fine-grained or glassy fault rocks believed to reflect earthquake-related frictional melting, are abundant in regions where pristine granulites show a transition to areas affected by Caledonian metamorphism (Figure 3b). Pseudotachylytes are located along highly localized faults cutting through the granulites (Austrheim & Boundy, 1994; Figures 4a and 4b). Such faults show single rupture displacements of up to 2 m (Petley-Ragan et al., 2019). The fault wall rocks locally display intense fragmentation in millimeter- to centimeter-thick zones around the fault planes, often without significant shear strain, followed by healing processes through grain growth and incipient metamorphism, including the formation of hydrous phases such as amphibole, micas, and clinozoisite (Petley-Ragan et al., 2018, 2019). Infiltration of hydrous fluids was thus directly coupled to the seismic slip.

The seismic faulting probably took place during different stages of the tectonic history of the Lindås Nappe as some pseudotachylytes recrystallized to an assemblage interpreted to have formed at ~ 680 °C, 1.5 GPa (Bhowany et al., 2018), while others recrystallized at ~600 °C, 1.0 GPa (Jamtveit, Moulas, et al., 2018). The corresponding pseudotachylytes (referred to as high-P,T and low-P,T pseudotachylytes in the following), wall rock damage, and incipient metamorphism are described in the following.

### 3.2. Pseudotachylytes

Figure 4 shows faults with associated pseudotachylytes formed around 1.5 and 1.0 GPa, respectively. The high-P,T pseudotachylytes are characterized by sharp contacts to the wall rocks (Figure 4a), abundant dendritic garnet crystals (Figure 4b; Austrheim & Boundy, 1994) in a fine-grained (<100 μm) matrix of kyanite, omphacite, plagioclase, K-feldspar, zoisite, rutile, and sometimes minor amounts of quartz and sulfides (Bhowany et al., 2018). Injection veins into the wall rocks are common and an increasing number of smaller garnets occur toward the pseudotachylyte margins where the cooling rate of the frictional melt was highest
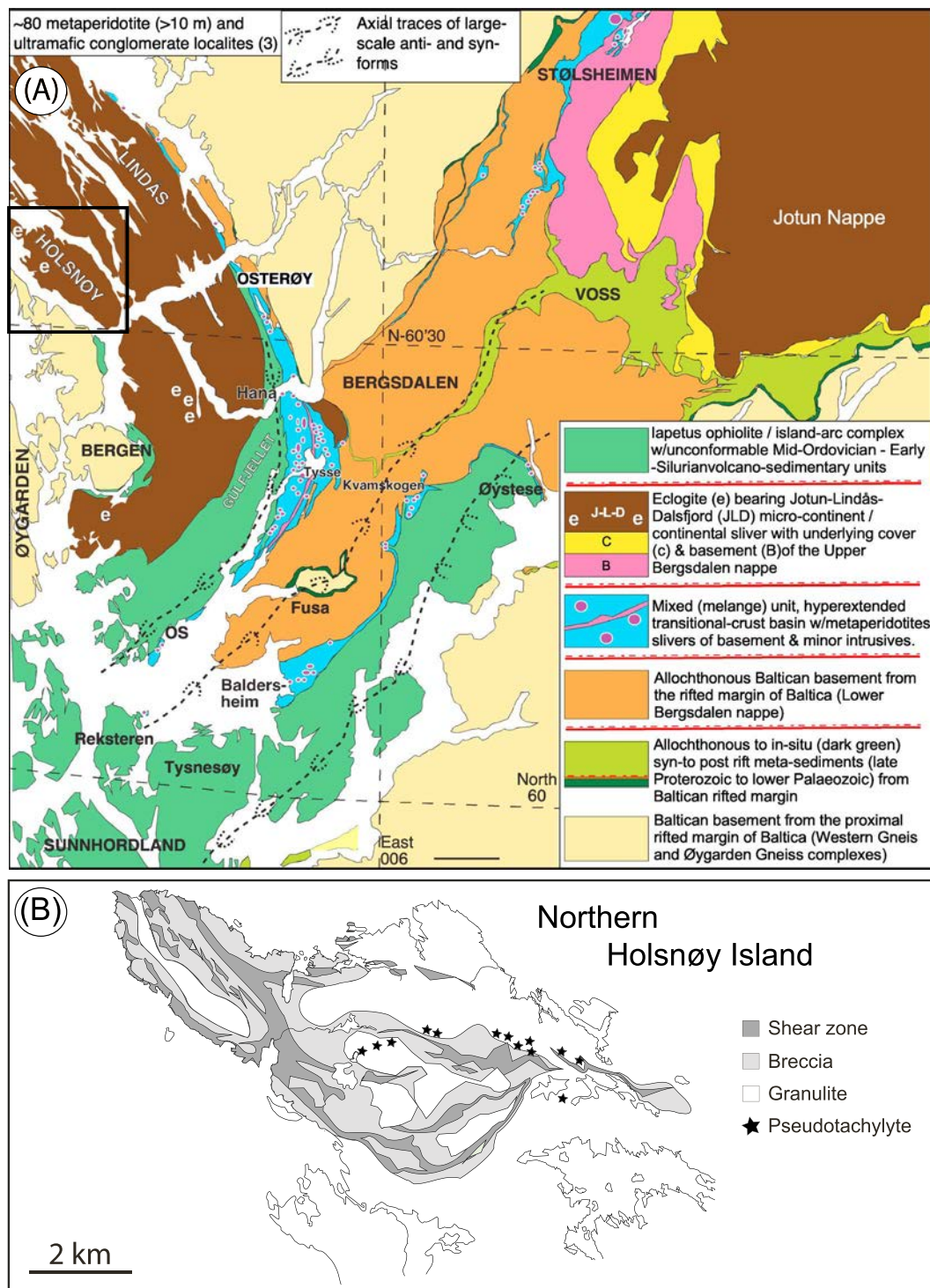
**Figure 3.** (a) Simplified map of the Caledonides of the Bergen-Jotun area in western Norway. The map shows the main tectonic units and the location of the eclogite bearing rocks studied in Holsnøy and their distribution in the Lindås-Jotun Nappe Complex (modified from Andersen et al., 2012). (b) Distribution of pseudotachylyte at Holsnøy, Bergen Arcs. Note that they are concentrated near the transition from the original Proterozoic granulites to the areas converted to eclogite and amphibolite facies rocks in shear zones and breccias.
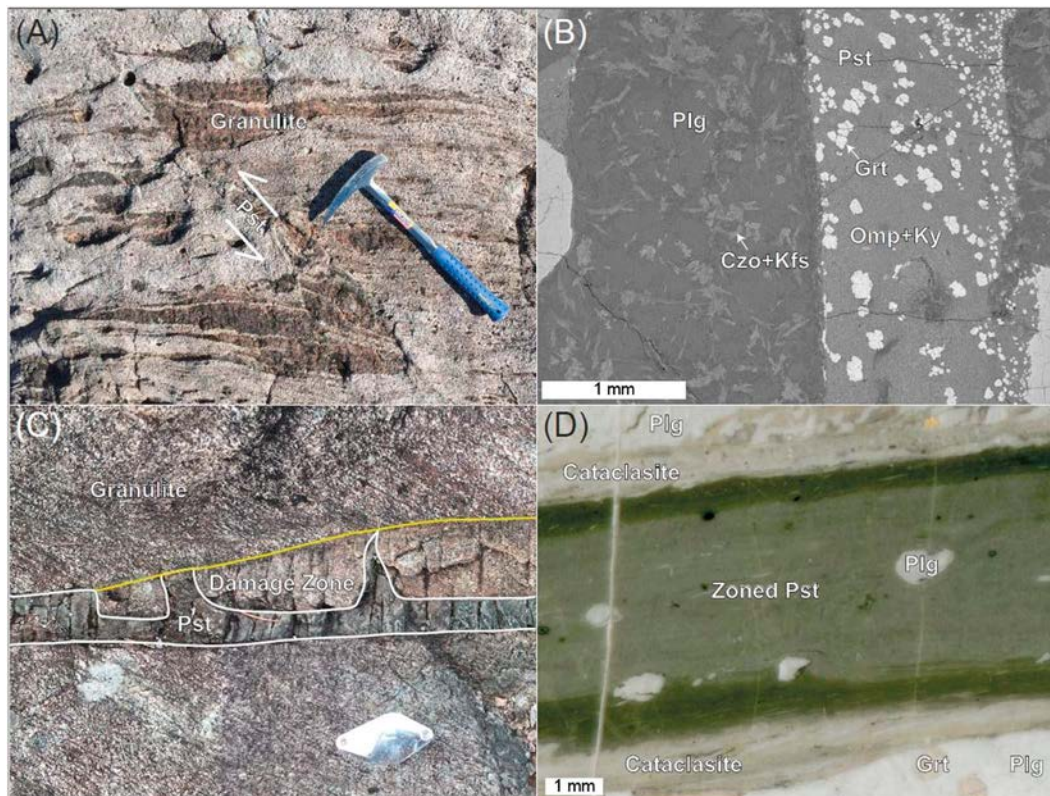
**Figure 4.** Faults and pseudotachylytes from the Bergen Arcs. (a) Fault with pseudotachylyte reflecting high-P,T conditions. (b) Corresponding interface between pseudotachylyte (pst) rich in dendritic garnet crystals and plagioclase rich wall rock. Note the small grain size near the wall. (c) Fault with pseudotachylyte and damage zone formed at low-P,T conditions. Pseudotachylyte injection veins cut the damage zone. (d) Close up of the pseudotachylyte, showing internal zoning and development of cataclastic layer in the wall rock. Abbreviations: Plg = plagioclase; Grt = garnet; Czo = clinozoisite; Ky–kyanite; Omp = omphacite; Kfs = K-feldspar; Pst = pseudotachylyte.

(Clerc et al., 2018). Thermal modeling suggests that the frictional melt solidifies within a timescale of seconds to minutes at most, depending on melt thickness.

A fault formed at the low-P,T condition was recently described by Petley-Ragan et al. (2019). This fault shows an offset of ~2 m (Figure 4c) and is filled by a ~1-cm thick and zoned pseudotachylyte rimmed by a 1- to 5-mm-thick layer of cataclastically deformed wall rock (Figure 4d). The inner pseudotachylyte comprises plagioclase microlites and clinozoisite symplectites, often aligned in flow bands suggesting flow of melt prior to crystallization. Other phases include kyanite, quartz, hornblende, K-feldspar, and anorthite. The outer pseudotachylyte consists of dark microcrystalline plagioclase and hornblende. Kyanite, K-feldspar, quartz, biotite, and carbonates are also found within the outer pseudotachylyte along with rare dendritic grossular-rich garnet. The presence of hydrous minerals and carbonates within the pseudotachylyte suggests postseismic partial recrystallization during fluid-induced metamorphism. Fragments of the cataclasites are found within the outer pseudotachylyte. In addition to the cataclasites zone, there is a locally developed wedge-shaped damage zone that extends up to 6 cm into the wall rocks on one side of the fault (Figure 4c). Damage zones are characterized by brittle deformation of the wall rocks, but in contrast to the case for the cataclasites, the shear deformation is very limited. Importantly, injection veins of pseudotachylyte are observed to intrude these damage zones (Figure 4c).

### 3.3. Wall Rock Damage

Wall rocks adjacent to both high-P,T and low-P,T faults show examples of extensive fragmentation with very limited shear strain, often referred to as *pulverization* when described from the shallow seismogenic regime (Mitchell et al., 2011; Muto et al., 2015; Rockwell et al., 2009; Wechsler et al., 2011). This pulverization was described from the high-P,T faults by Austrheim et al. (2017), and Petley-Ragan et al. (2018) and from a low-P,T fault by Petley-Ragan et al. (2019).
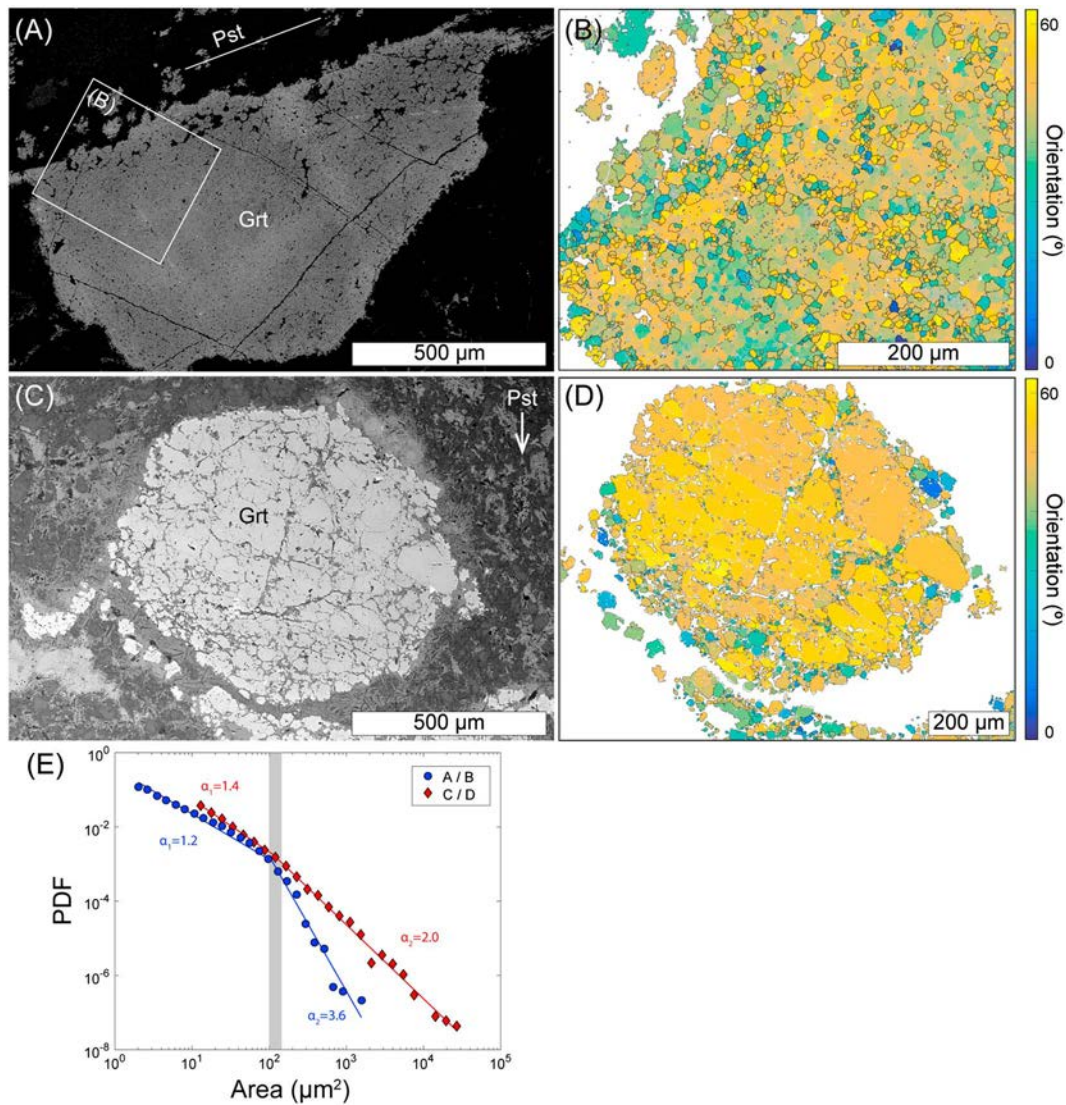
**Figure 5.** Wall rock garnets. (a) Garnet cut by high-P,T pseudotachylyte showing no or very limited shear strain. Note abundant inclusions. (b) Orientation map of the garnet in (a) showing a large number of grains and subgrains with a strong crystallographic preferred orientation (CPO) inherited from the host granulite garnet. (c) Garnet from the damage zone next to the low-P,T pseudotachylyte in Figure 4c. The euhedral crystal shape is preserved despite extensive brittle fragmentation. (d) Orientation map of the garnet in (c), again showing a strong CPO inherited from the host. Low-angle grain boundaries (<10°) are gray and high-angle grain boundaries (≥10°) are black. (e) Probability density function (PDF) of the area of grains defined by low-angle boundaries in b) in blue, and d) in red. Gray bar denotes the scale at which there is a cross-over to lower power law exponents for small grains (see Aupart et al., 2018 for methods and discussion of the significance of the cross over scale).

Fresh, granulite facies, wall rock garnets are chemically homogeneous with a very low content of mineral inclusions. Figure 5 shows the contrasting alteration observed in wall rock garnets from the two situations described above. One garnet cut by the high-P,T pseudotachylyte (Figure 5a) experienced pervasive fragmentation into grains and subgrains (Figure 5b) with a mean grain size of 31 $\mu m^2$ (sample AF2-4 of Aupart et al., 2018) and a strong crystallographic preferred orientation (CPO; J- and M-index values of 6.0 and 0.3 respectively, cf. Mainprice et al., 2015). Grains larger than the median size show a power law probability distribution with a large (negative) exponent (−3.6, Figure 5e), reflecting a very narrow grain size distribution. Grain boundaries are dominated by triple junctions and 120° angles (Aupart et al., 2018), reflecting significant recovery and grain growth in the wake of the fragmentation process. The fragmented garnet furthermore contains a large number of inclusions distributed along the grain boundaries and triple junctions of the new grains and subgrains, occupying in total ~7% of the garnet volume (Austrheim et al., 2017).
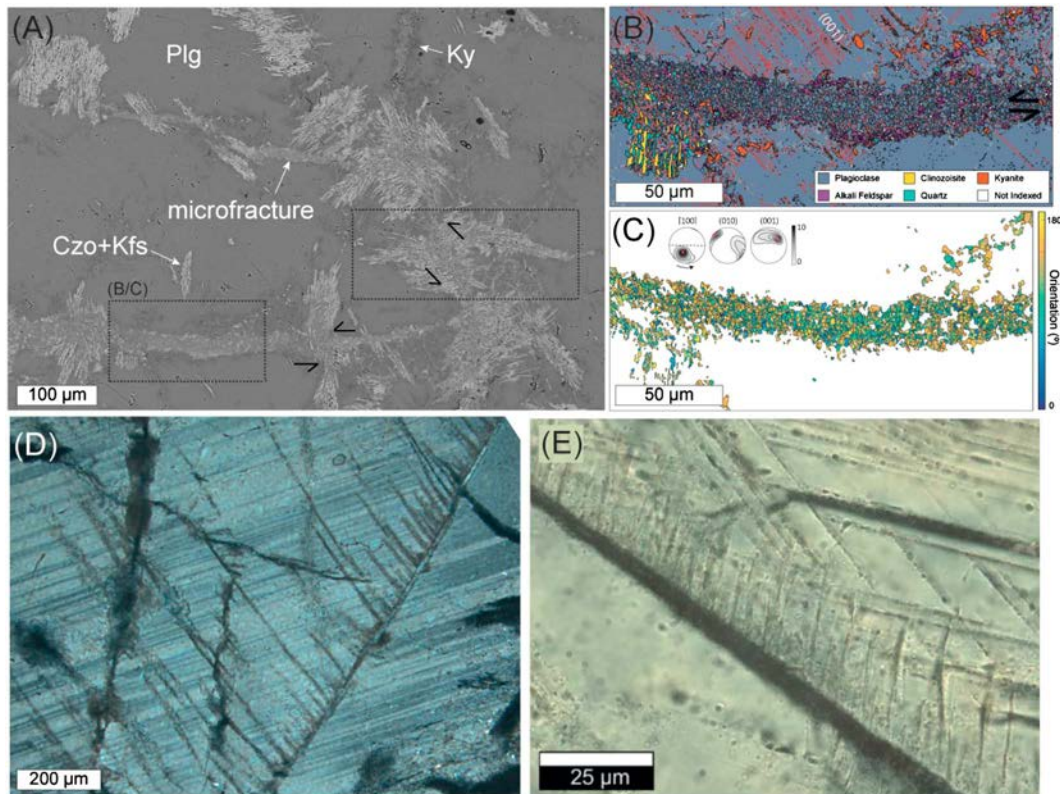
**Figure 6.** Plagioclase microfractures. (a) Backscatter electron image of a plagioclase (Plg) grain 1 mm from an eclogite facies pseudotachylyte. Microfractures with thicknesses of up to 50 μm are spatially associated with clinozoisite (Czo), quartz (Qtz), alkali feldspar (Kfs), and kyanite (Ky). (b) Phase map of a microfracture in (a). The grains have high-angle grain boundaries (black) and few twin boundaries (red), while the host plagioclase on either side of the microfracture contains low-angle grain boundaries (gray). (c) The orientation of the plagioclase grains within the microfracture is inherited from the host orientation (red points in the pole figures) with minor top-to-the-left shear. (d) Cross-polarized light image of asymmetrical secondary fracturing in plagioclase 2 cm from a microshear zone on Holsnøy. (e) Feather features in shock metamorphosed quartz from Poelchau and Kenkmann (2011).

Granulite facies garnets from the damage zone 1.5 cm from the low-P,T pseudotachylyte, on the other hand, clearly display brittle fracturing while keeping their euhedral crystal shape (Figure 5c) in a situation with very low shear strain and fragment rotation (Figure 5d). The same applies to clinopyroxene grains (Petley-Ragan et al., 2019). In this case the mean fragment size (for garnet) is 160 μm$^2$, and the power law distribution for both garnet and pyroxene fragments has a slope of ~ −2 (Figure 5e), similar to the scaling behavior previously reported from pulverized wall rocks close to the fault core of shallow seismic faults (Muto et al., 2015). Inclusions in this garnet are concentrated along brittle fractures, some of which extend through a major fraction of the garnet crystal (Figures 5c and 5d). The CPO is weaker than for the garnet described above with J- and M-index values of 3.4 and 0.15, respectively.

The granulites at Holsnøy are dominated by plagioclase-rich lithologies, and the pseudotachylyte-producing faults also produce abundant microfracturing of the typically very coarse-grained plagioclase-rich wall rocks. Petley-Ragan et al. (2018) describe how micro-fractures in wall rocks around high-P,T pseudotachylytes are filled with fine-grained clinozoisite, kyanite, K-feldspar, and quartz and aggregates of plagioclase (grain diameter around 1 μm or even less) formed by fragmentation of the original grains with very limited shear strain (Figures 6a–6c). The new grains inherit the crystallographic orientation of the host (Figure 6c) and show a strong shape-preferred orientation with the long axis parallel to the fault slip surface, irrespective of the orientation of the microfracture in which they formed (Petley-Ragan, 2018). This suggests that the grains formed at a stage where thermal, stress or other gradients caused by the earthquake were still significant. If thermal gradients were the controlling factor, the new plagioclase grains must have formed within timescales of seconds to minutes after the fault slip (Clerc et al., 2018).
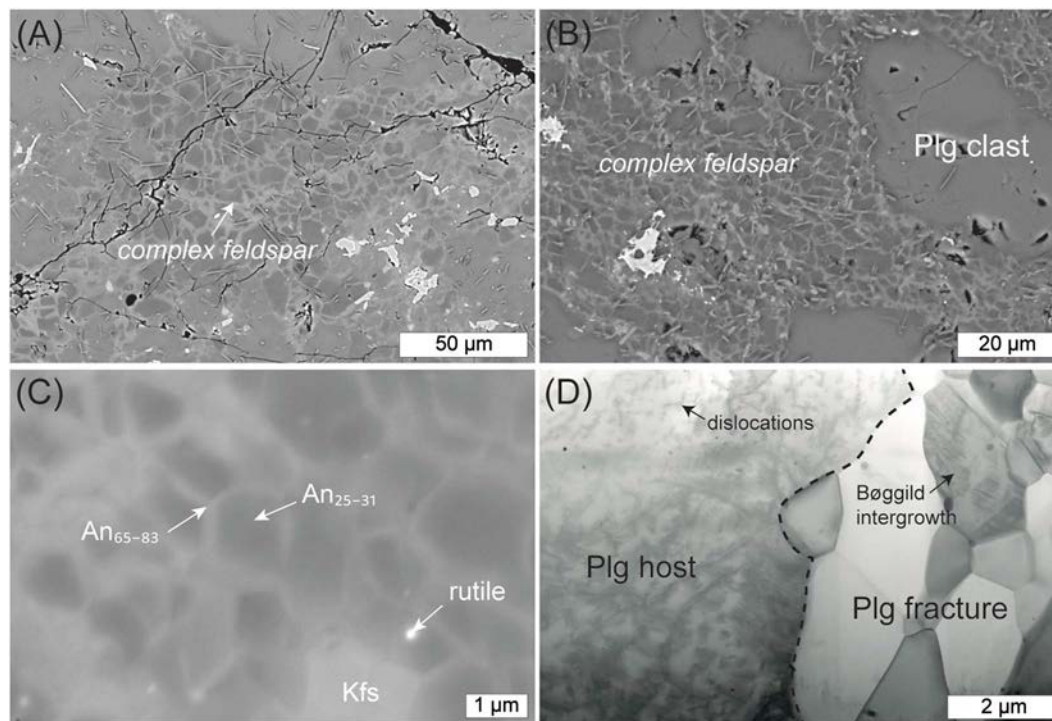
**Figure 7.** Complex feldspar microstructures. (a) Backscatter electron image of plagioclase in the wall rock adjacent to high-P,T pseudotachylyte. The microstructure consists of albite-rich grains with anorthite-rich rims. (b) Backscatter electron image of the matrix of cataclasite adjacent to a low-P,T pseudotachylyte (Figure 4d). (c) Backscatter electron image of grains within a microfracture adjacent to a high-P,T pseudotachylyte (Figure 6b). (d) Combined bright field and high-angle annular dark field image of the plagioclase host and the grains within the microfracture (Figure 6b). The host is rich in dislocations while the grains are dislocation-free and locally display intimate feldspar intergrowths.

Some of the micro (shear-) fracture in plagioclase furthermore show secondary development of tensile fractures with a characteristic angle to the host fracture (Figure 6d). These fractures develop asymmetrically, on only one side of the host fracture and are very similar to feather features produced by low shock metamorphism in quartz during meteorite impacts (Figure 6e; Poelchau & Kenkmann, 2011). Similar features have also been produced during dynamic rupture experiments in analog materials, where the ruptures travel near the shear wave velocity (Griffith et al., 2012). The asymmetrical features therefore likely represent the fast propagation of microfractures in the wall rocks of earthquake slip planes which produce locally high stresses within their vicinity, causing tensile fracturing (Petley-Ragan et al.2018). Feather features in plagioclase are observed associated with both high and low-P,T pseudotachylytes, and similar features have been observed in other minerals, including scapolite. The fine-grained plagioclase aggregates often display a characteristic chemical zoning with Na-rich cores ($An_{25-31}$) and Ca-rich ($An_{65-83}$) rims (Figures 7a–7c, Petley-Ragan et al., 2018) with some grains displaying intimate feldspar intergrowths (Figure 7d). A very similar microstructure was described from amphibolite facies shear zones by Mukai et al. (2014) and ascribed to unmixing of the plagioclase near the Bøggild miscibility gap followed by fluid- and stress-induced coarsening of the intergrowth. Grain boundary sweeping coupled with dissolution-precipitation then forms the fine-grained aggregate with Ca-rich zonation (Mukai et al., 2014). This microstructure was described as "complex feldspar" by Mukai et al. (2014). The microstructures characterizing damaged wall rock plagioclase around low P,T-pseudotachylytes are very similar to the structures for high-P,T pseudotachylytes (Cf. Figures 7a and 7b). Abundant microfracturing with fragmentation and formation of complex feldspars is observed. Fine-grained plagioclase grains are essentially dislocation free, while the host feldspar has a high density of dislocations (Figure 7d), yet the new grains inherit the crystallographic orientation of the host.

### 3.4. Incipient Metamorphism of Wall Rocks

Wall rock damage around pseudotachylyte-bearing faults is always associated with incipient metamorphism along fractures and grain boundaries. Additionally, the granulite facies plagioclase often develops a "cloudy" interior due to the growth of small inclusions. The mineral assemblage forming in fault wall rocks is very
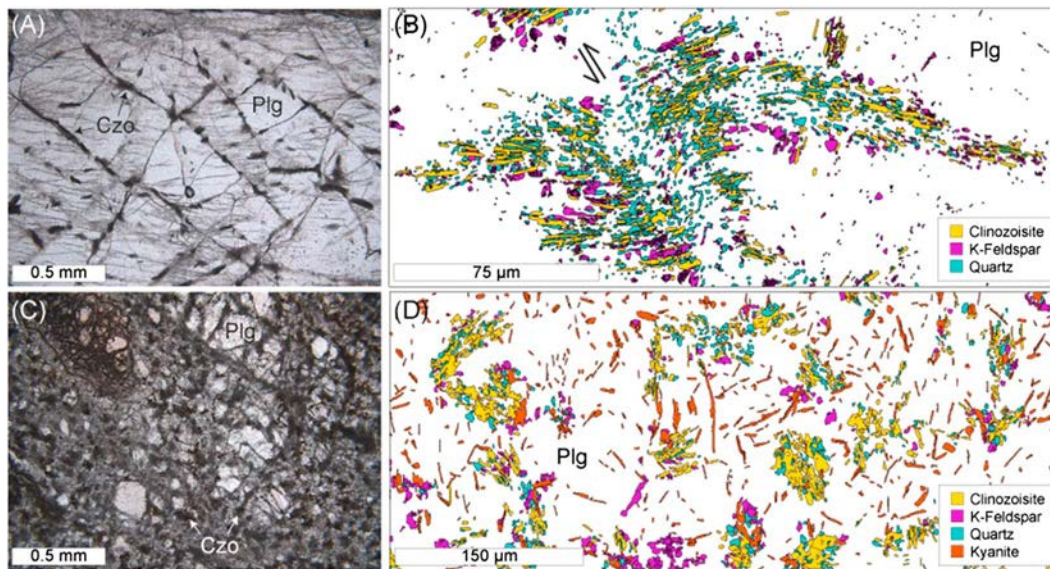
**Figure 8.** Incipient plagioclase metamorphism. (a) Plane polarized light image of fractured wall rock plagioclase around a high-P,T pseudotachylyte. (b) Phase map of an intergrowth of clinozoisite, quartz and K-feldspar associated with a microfracture at eclogite facies (see Petley-Ragan et al., 2018). (c) Plane polarized light image of fragmented plagioclase from an asymmetrical fault damage zone from a low-P,T pseudotachylyte. (d) Phase map of the distributed clinozoisite-quartz intergrowths, K-feldspar grains and kyanite crystals from an area in (c).

similar for both high-P,T and low-P,T pseudotachylytes (Figure 8). Fractures in the original plagioclase domains show growth of fine-grained clinozoisite, kyanite, quartz, and K-feldspar. During this process, the remaining plagioclase becomes more Na-rich. The incipient stages of metamorphism clearly take place within the stability field of albite. The reaction

$$\text{Anorthite} + H_2O = \text{Zoisite} + \text{Kyanite} + \text{Quartz}$$
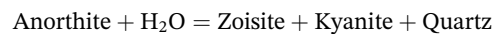
limits the pressure to 0.7–1 GPa in the temperature range 600–700 °C for pure phases (Koziol & Newton, 1988). Given that the plagioclase and the fluid are not pure end-member phases, these are minimum estimates for the pressures. The fluid-absent breakdown of anorthite to grossular-kyanite-quartz is expected above ~1.5 GPa at 700 °C (Koziol & Newton, 1988) but is not observed. Equilibrium considerations thus suggest that all pseudotachylyte-bearing faults formed under pressure conditions in the range 1–1.5 GPa, which is also consistent with the stability of Ab-rich plagioclase. Mass balance calculations show that the abundant K-feldspar in the wall rocks requires that this component was introduced with the metamorphic fluids (Petley-Ragan et al., 2018). Heterogeneous stress fields have additionally been suggested to influence the reaction products in plagioclase microfractures due to their orientation relative to the principle stress direction (Moore et al., 2019). Finally, the absence of both phengite and paragonite in the majority of microfractures during incipient metamorphism indicate that the activity of water was low, probably below ~0.1 (Petley-Ragan et al., 2018), possibly due to water consuming reactions in wall rocks characterized by low fluid/rock ratios.

Interestingly, the progress of metamorphism in fractured wall rocks is often higher in wall rocks adjacent to high-P,T pseudotachylytes. As discussed below, the progress of metamorphic reactions may have implications for the generation of local pressure increases through the associated mechanical weakening that hydration reactions invariably cause.

## 3.5. Initiation of Shear Zones

The reduction in grain size and rheological weakening associated with damage and fluid-driven metamorphism leads to postseismic localization of shear strain. The development of asymmetric damage zones, such as the one shown in Figure 4c, may lead to a subsequent asymmetry during shear strain localization. In the following, we will describe a low-P,T pseudotachylyte-bearing fault that shows such an asymmetry during the early stages of shear zone development. The wall rocks are granulite facies anorthosite with
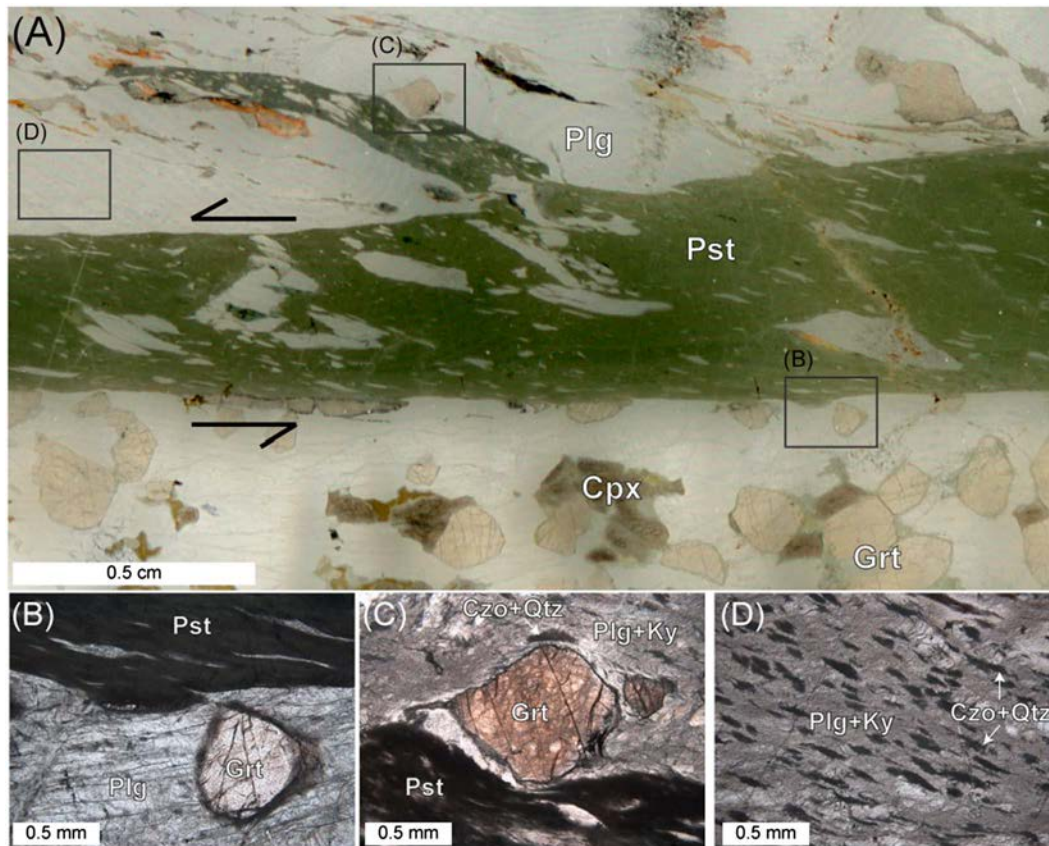
**Figure 9.** Sheared pseudotachylyte with asymmetric wall rock damage and alteration. (a) Thin section scan of an amphibolite facies pseudotachylyte in granulite facies anorthosite from the Bergen Arcs. (b) Plane polarized light image of comparatively unreacted plagioclase and garnet in the lower wall rock. (c) Plane polarized light image of plagioclase and garnet in the upper wall rock. Plagioclase has reacted to clinozoisite, quartz, kyanite, and fine-grained plagioclase. (d) Plane polarized light image of plagioclase in the upper wall rock that has fully reacted to fine-grained products and illustrates shear through elongated clinozoisite-quartz intergrowths.

plagioclase, garnet and clinopyroxene. The pseudotachylyte has a matrix of plagioclase, amphibole, biotite, K-feldspar, and kyanite with symplectites of clinozoisite and quartz. Garnet dendrites are only present near the margin of the pseudotachylyte vein and within injection veins. Elongate plagioclase clasts within the pseudotachylyte are oriented 10–20° from the strike of the fault illustrating a top-to- the-left sense of shear across the fault (Figure 9a). The plagioclase clasts are largely made up of equidimensional grains <10 $\mu$m in size. Such fine-grained aggregates clearly localize strain creating aspect ratios >5 compared to plagioclase clasts in the previously described pseudotachylytes which have aspect ratios ≤2 (Figure 4d). The complex feldspar microstructure is a dominant feature within the clasts and the pseudotachylyte matrix. The original granulite facies fabric is relatively intact on one side of the fault (lower part of Figre 9a). Here, fractures and grain boundaries are closely associated with fine-grained reaction products (Figure 9b). The other side of the fault shows signs of brittle damage (upper part of Figure 9a). Most notably is the presence of an undulating injection vein with an orientation approximately parallel to the elongated clasts in the pseudotachylyte (Figure 9a). One-sided veins are attributed to the injection of melt into cracks in the wall rock that experienced tensile stress and extensive damage during dynamic earthquake rupture (Di Toro et al., 2005). Garnet on this side of the fault is highly fragmented and displays a yellow to brown discoloration but does not show a high degree of metamorphic reaction (Figure 9c). Plagioclase is also highly fractured and locally completely replaced by reaction products. In many places, the grain size of plagioclase has been reduced to <10 $\mu$m creating regions of fine-grained plagioclase aggregates that again display the complex feldspar microstructure. Elongated clinozoisite-quartz symplectites illustrate the localization of shear strain within plagioclase regions of the upper wall rock (Figure 9d). This is very different from the more isotropic microstructures observed in the
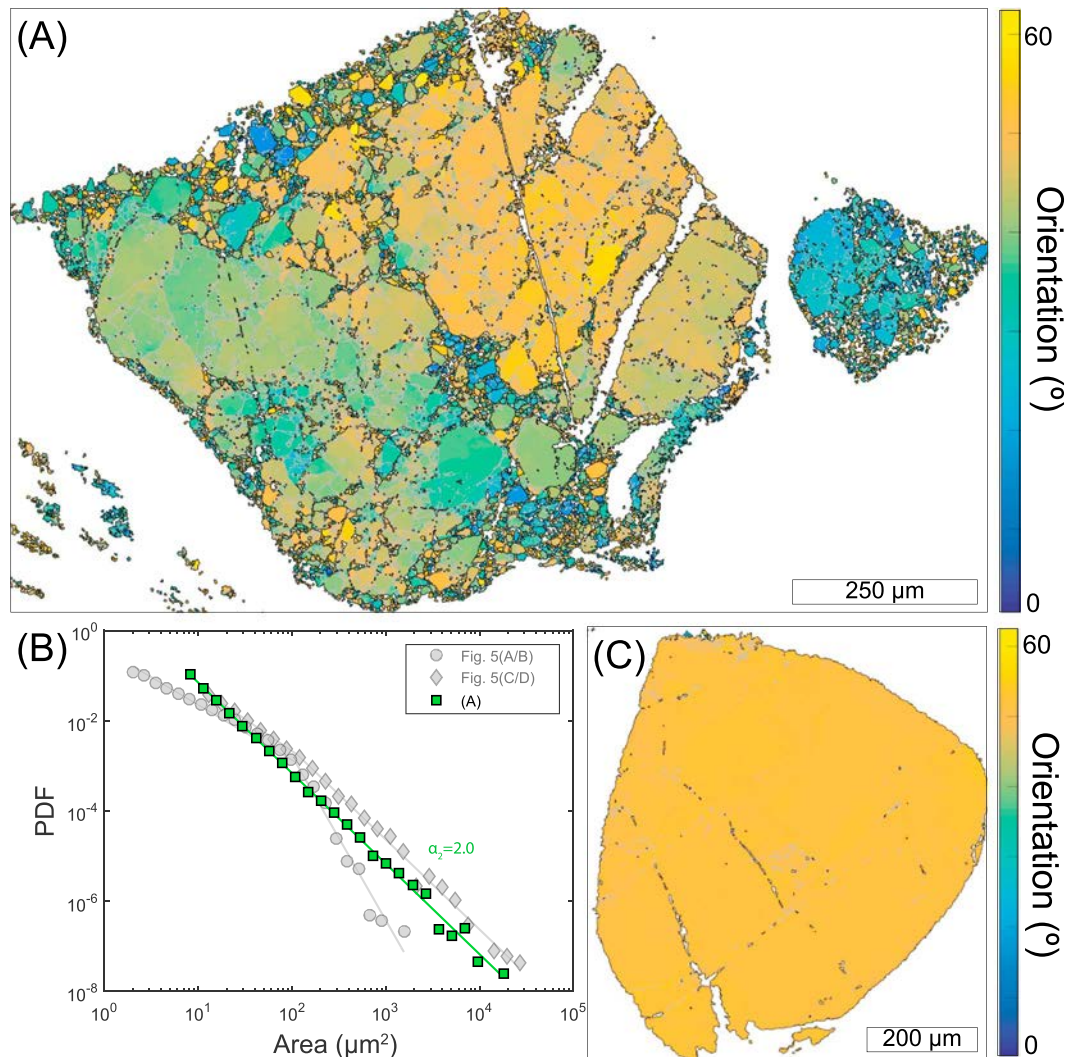
**Figure 10.** Contrasting wall rock garnets from Figure 9. (a) Orientation map of the garnet from the upper wall rock of Figure 9a. Fragments are defined by low-angle grain boundaries with misorientations >1° and <10° (gray) and high-angle grain boundaries with ≥10° misorientation (black). (b) Probability density function of the area of garnet fragments defined by low-angle grain boundaries in (a). (c) Orientation map of the garnet from the lower wall rock of Figure 9a. Few low-angle grain boundaries (gray) are present within the grain.

plagioclase-rich domains of the asymmetrical damage zone described in Figures 8c and 8d. Microstructures indicative of shear strain are absent in the lower wall rock of the pseudotachylyte shown in Figure 9a.

Two garnets on either side of the pseudotachylyte were analyzed with electron backscatter diffraction (Figures 10a and 10c). The garnet in the upper wall rock of Figure 10a is made up of many fragments defined by ≥1° misorientations. These fragments fit a power law grain size (area) distribution with slope −2.0 over more than 4 orders of magnitude (Figure 10b). This is identical to the scaling behavior of the fragmented ("pulverized") garnet from both the asymmetrical damage zone described in Figure 5c and from pulverized rocks around faults in the normal seismogenic regime (Muto et al., 2015). The garnet grain in the lower wall rock of Figure 9b has few internal misorientations but remains intact as a single grain (Figure 10c).

### 3.6. Rheological Change and Eclogitization

From the incipient stages described above, the shear zones at Holsnøy evolve in stages where the microstructures and fabric from the early stages of their formation are completely obliterated (Austrheim, 1987). However, relict pseudotachylyte fragments can occasionally be observed embedded within the shear zones (Jamtveit, Ben-Zion et al., 2018). During shear zone development and continued hydration of the granulites,
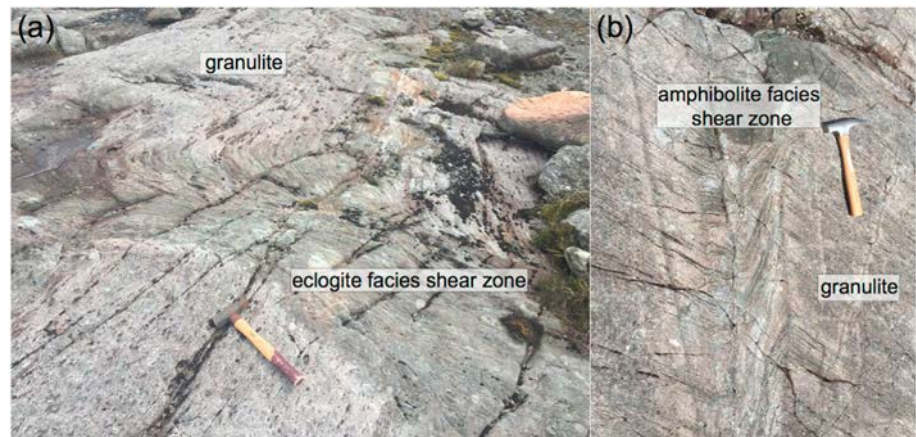
**Figure 11.** (a) Well-developed shear zone with a plagioclase-absent eclogite facies mineralogy and (b) a less extensively developed amphibolitized shear zone where the original granulite facies layering can still be traced across the zone.

both the associated grain size reduction and the formation of sheet silicates lead to a pronounced reaction-induced weakening. The introduction of fluids furthermore allows diffusion creep as an additional deformation mechanism which will facilitate effective deformation even under the relatively lower stress conditions. All these factors may contribute to the transition from brittle deformation of the strong granulites to the ductile flow of the weaker hydrated product rocks (Figure 11).

Interestingly, Bhowany et al. (2018) showed that during shear zone development from the high-P,T pseudotachylytes, the rocks may evolve into a plagioclase-free eclogite facies mineralogy which apparently equilibrated at a pressure of 2.1–2.2 GPa, around 0.5 GPa higher than the pressure estimates of the recrystallized pseudotachylytes, but still at the same temperature (~680 °C). Traditionally, this would have been interpreted to reflect post-seismic burial from a depth of 50–55 km during pseudotachylyte formation, to 70–75 km during eclogitization. However, Jamtveit, Moulas, et al. (2018) pointed out that nearly 20 km of isothermal burial is thermomechanically unfeasible, and suggested that the increased pressure may rather be due to local weakening induced by the hydration reactions. The principle behind generation of "overpressure" (pressure in excess of lithostatic) in a weak inclusion was outlined by Mancktelow (1993, 2006, 2008)

and is illustrated in Figure 12. For a lower crustal lithostatic (confining) pressure of 1.5 GPa, the differential stress required for brittle failure of dry granulite is probably at least 1 GPa (cf. Kohlstedt et al., 1995); hence, an overpressure of 0.5–0.7 GPa is realistic.

The P,T-conditions of the amphibolite facies shear zones that develop around the low-P,T pseudotachylytes are not very well constrained and may possibly vary significantly. Available amphibolite facies mineral assemblages for amphibolite facies shear zones as well as amphibolitic hydration zones around late pegmatites through the granulites both indicate conditions around 1 GPa and 600 °C (Kühn, 2002; Jamtveit, Moulas, et al., 2018).
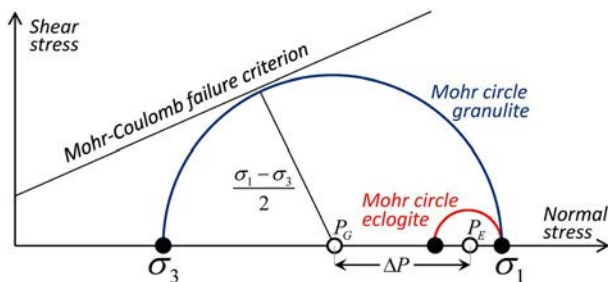
## 3.7. Fluid Source and the Timescale of Metamorphism

The aqueous fluids that were introduced with the earthquakes and drove retrograde metamorphism at Holsnøy had a salinity in the range 5–50 wt% NaCl and variable $CO_2$ and $N_2$-content. They were most likely derived from a source external to the host granulites (VanWyck et al., 1996) which only contain rare $CO_2$-rich inclusions (Andersen et al., 1991), and experienced increasing salinity as the water was consumed by hydration reactions (Svensen et al., 1999).

Attempts to date the fluid introduction and retrograde metamorphism have given mixed results. U-Pb geochronology on eclogite assemblages



**Figure 12.** Representative Mohr circles for a weak eclogite inclusion embedded into a strong granulitic matrix. Force balance between inclusion and matrix requires that the total stress normal to the inclusion-matrix interface must be identical in the inclusion and the matrix. The total stress is the sum of the pressure and the deviatoric stress. Since the deviatoric stress is smaller in the weak inclusion than in the strong matrix, the pressure in the weak inclusion ($P_E$) must be correspondingly larger than the one in the matrix ($P_G$) to obtain the same total stress. In detail, the pressure variation depends on the aspect ratio of the inclusion and its orientation with respect to the applied differential stress (Moulas et al., 2014). However, the "overpressure" in the inclusion may reach values in the range 50–70% of the differential stress ($\sigma_1 - \sigma_3$), depending on the magnitude of the intermediate stress ($\sigma_2$; Jamtveit, Moulas, et al., 2018).
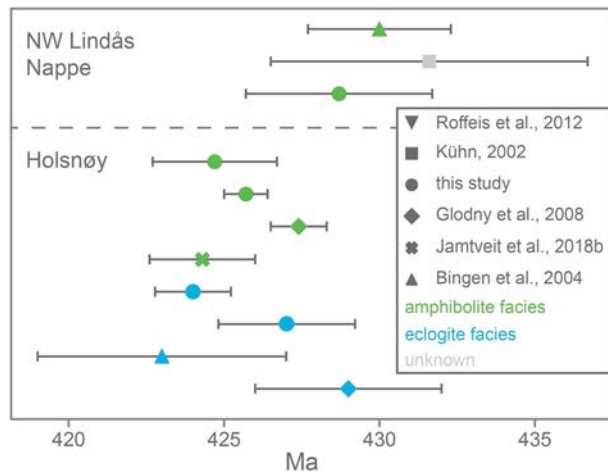
**Figure 13.** Compilation of $^{206}Pb/^{238}U$ ages of zircons from veins and pegmatites associated with amphibolites and eclogites from the Lindås Nappe of the Bergen Arcs. The age from Jamtveit, Moulas, et al. (2018) has been adjusted from 423.6 $\pm$ 1 to 424.3 $\pm$ 1.7 Ma after an improvement of the laboratory blank correction

by Bingen et al. (2004) gave 423 $\pm$ 4 Ma, slightly younger than the U-Pb age obtained by Glodny et al. (2008) (429 $\pm$ 3 Ma), while Glodny et al. (2002) obtained an eclogite age of 422 $\pm$ 10 Ma by the Sm-Nd method, and 425 $\pm$ 4 Ma by the Rb-Sr method. The amphibolite facies metamorphism has previously been assumed to have occurred at 410–415 Ma based on Rb-Sr results (Glodny et al., 2008), but Jamtveit, Moulas, et al. (2018) reported a U-Pb age of 423.6 $\pm$ 1.0 Ma for a late micarich pegmatite causing amphibolitization of granulites. To test and complement these result, we have carried out additional U-Pb dating of zircons from a range of pegmatites from Holsnøy, some of which cause amphibolitization of the original granulites while others form during eclogite formation (see supporting information for analytical methods and Figure S1 for presentation of new data and a U-Pb concordia diagram). The results are summarized in Figure 13. The results from Holsnøy are essentially identical within errors. Eclogite facies and amphibolite facies pegmatites show overlapping ages with a mean of 425.6 ($\pm$2.0) Ma for pegmatites without an obvious Proterozoic precursor. The maximum duration of fluid induced metamorphism at Holsnøy based on these data is probably within ca 5 Myr, comparable to the timescale of eclogitization of the lower crust of India during subduction under Tibet (~ 6 Myr, Hetényi et al., 2007).

## 4. The Lofoten Area

To illustrate that the observations from the Bergen Arcs are not unique, we will in the following present observations from the Lofoten-Vesterålen archipelago, some 1,000 km further north in the Norwegian Caledonides (Figure 14). In this region, the basement lithologies are predominantly composed of Archaean to Paleoproterozoic orthogneiss and paragneiss, intruded at 1.9–1.7 Ga by a suite of anhydrous Anorthosite-Mangerite-Charnockite-Granite plutons (Corfu, 2004a). Pluton emplacement occurred under granulite facies conditions estimated at 750–800 °C and 0.4–1.2 GPa (Markl et al., 1998). The primary igneous texture and the anhydrous granulite facies mineral assemblages are generally well preserved in the Anorthosite-Mangerite-Charnockite-Granite suite.

Lofoten represents a tectonic window of basement rocks of the Baltica plate beneath the Caledonian nappe pile, in a similar tectonic position to the Western Gneiss Region in south- western Norway. The Lofoten basement rocks have largely escaped the Caledonian tectono-metamorphic overprint as the result of the limited availability of fluids necessary to facilitate viscous deformation of the anhydrous, strong granulites (Steltenpohl et al., 2004). Caledonian fabrics and structures are remarkably sparse and like in the case for the Lindås Nappe in the Bergen Arcs, they are typically localied in eclogite and amphibolite facies ductile shear zones. A number of studies consistently indicate that fracturing, pseudotachylyte formation and fluid infiltration were key processes for the nucleation of high temperature shear zones in the anhydrous rocks of Lofoten (Kullerud et al., 2001; Menegon et al., 2013; Menegon et al., 2017; Steltenpohl et al., 2006).

Pseudotachylytes generated at lower crustal conditions have previously been reported from three islands in Lofoten-Vesterålen: Flakstadøy (Nusfjord and Skagen:Menegon et al., 2017 ; Steltenpohl et al., 2006), Langøya (Eidsfjord: Plattner et al., 2003; Moecher & Steltenpohl, 2009, 2011;Leib et al., 2016 ; Steltenpohl et al., 2011), and Hinnøya (Fiskefjord: Moecher & Steltenpohl, 2011; Steltenpohl et al., 2011; Leib et al., 2016). However, a field survey carried out in connection with the present study revealed that they are probably far more abundant than hitherto recognized as they also occur on Vestvågøy and Moskenesøya (Figure 14). In all these cases, pseudotachylytes occur within anhydrous rocks such as anorthosites, monzonites, and gabbronorites.

The pseudotachylytes of Flakstadøya are generally coeval with mylonitic deformation; that is, they overprint and are overprinted by mylonites that formed under similar P,T-conditions (Steltenpohl et al., 2006; Menegon et al., 2017). In Nusfjord East (Figure 14), the P,T-conditions of formation and mylonitization of pseudotachylytes were estimated at 650–750 °C, 0.7–0.8 GPa (Menegon et al., 2017). The formation of pseudotachylytes in Flakstadøya was associated with fluid infiltration, and Menegon et al. (2017) estimated a
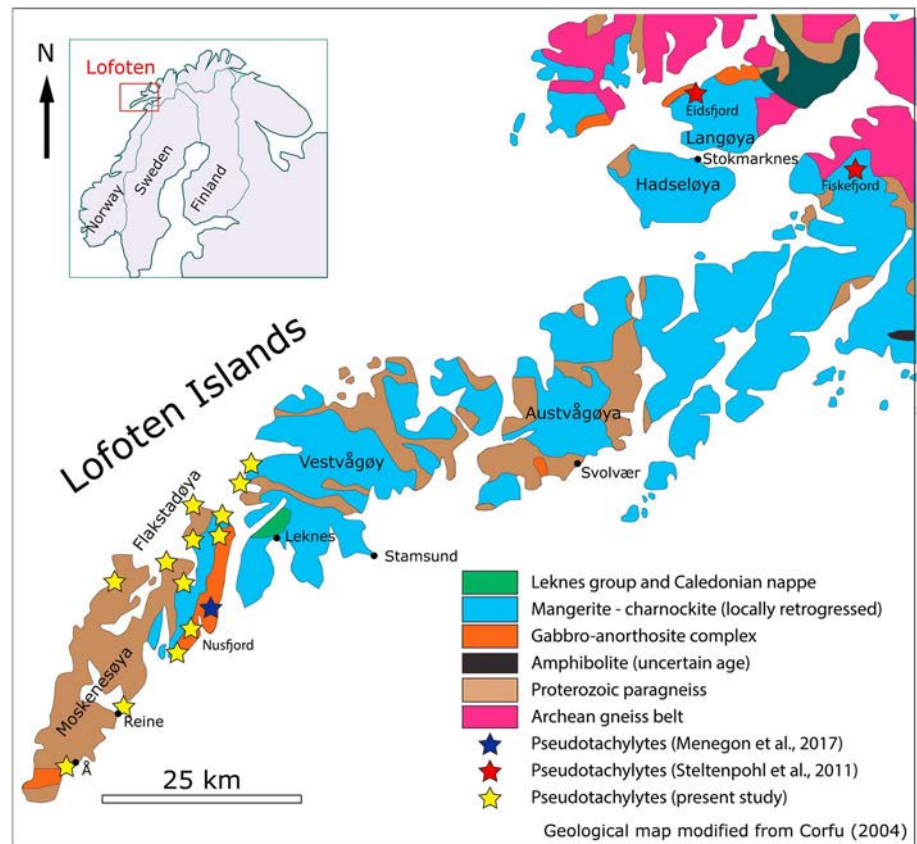
**Figure 14.** Map of the southern part of the Lofoten islands, located in northern Norway (inset). The locations of outcrops with pseudotachylytes are indicated with stars. The geological map is modified from Corfu (2004b) and shows the compositional variability in lower crustal rocks.

modest (0.2 wt%) increase in $H_2O$ content from the anorthosite host rock to the mylonitized pseudotachylytes (from 0.04 to 0.25 wt%). On eastern Moskenesøya, however, neither the pseudotachylytes nor their wall rocks show any evidence of fluid infiltration and instead preserve the dry, granulite-facies mineralogy.

High-grade pseudotachylytes in Eidsfjord and Fiskefjord have been attributed to post-Caledonian Devonian ductile extension localied on low-angle detachment faults. Several episodes of pseudotachylyte formation were found along both detachments faults, with many generations of pseudotachylytes being overprinted by mylonitic deformation (Steltenpohl et al., 2011; Leib et al., 2016). The P,T conditions of formation and mylonitization of pseudotachylytes in Eidsfjord and Fiskefjord were estimated at ~650 °C, 0.7 GPa and 650 °C, 0.95 GPa, respectively (Moecher & Steltenpohl, 2011).

In the following, we describe pseudotachylytes and transitions toward ductile shear zones in the Western parts of the Lofoten-Vesterålen archipelago.

### 4.1. Dry Pseudotachylytes on Moskenesøya

Several roadcuts along a distance of ~3 km on Moskenesøya close to Reine show pseudotachylytes with sharp contact to the wall rocks and without alteration halos or shear zone development (Figures 15a and 16a). The host rock consists almost exclusively of plagioclase with minor pyroxene and opaque minerals (Figure 15), except for one outcrop that consists of patches richer in pyroxene and amphibole (Figure 16). In both cases, the pseudotachylytes comprise wall rock clasts and a fine-grained mixture of feldspars and clinopyroxene. The clasts are often slightly sheared (Figure 19c). Dendritic garnets, some of which have euhedral overgrowths, are not sheared (Figure 16c). These observations suggest a temporal development in which wall rock fragmentation and shearing precedes the crystallization of melt-derived garnet. Sheared plagioclase clasts are surrounded and cut by bands of small plagioclase grains (Figure 15c). Close
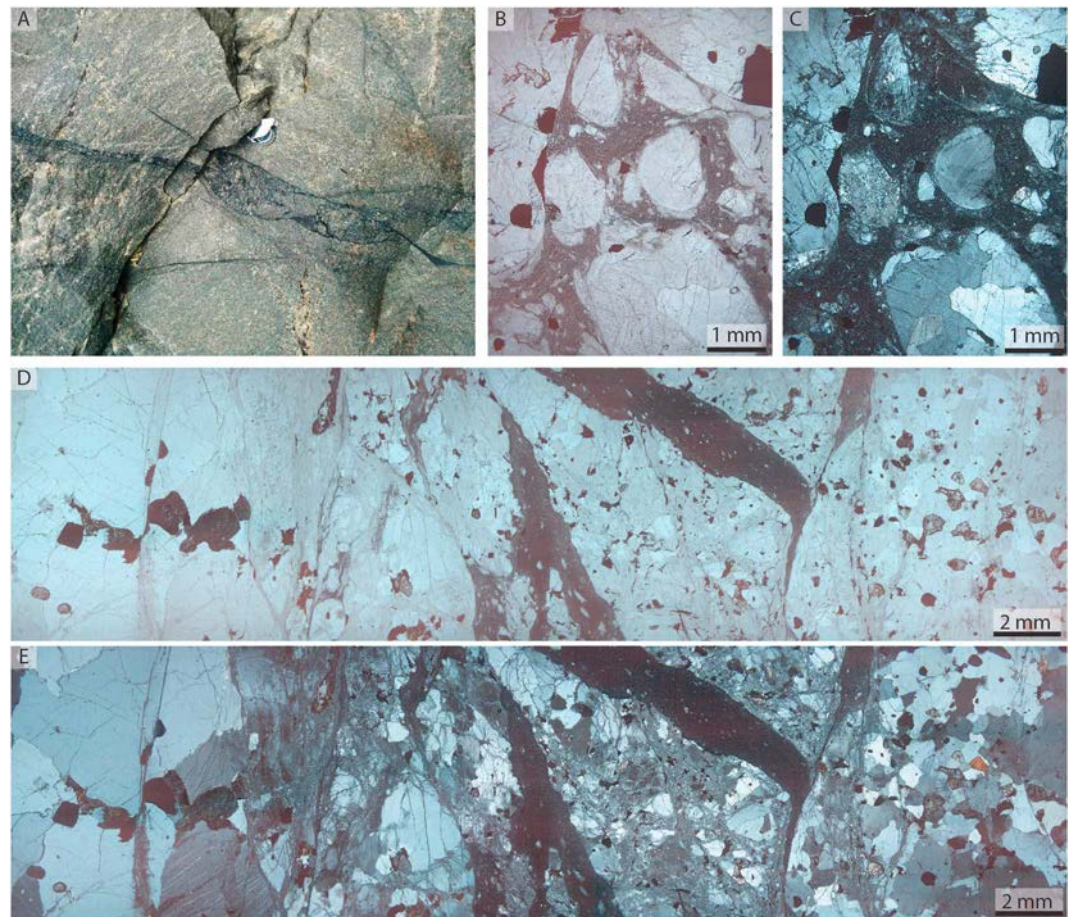
**Figure 15.** Dry pseudotachylytes on Moskenesøya. (a) Pseudotachylyte (dark) matrix surrounding breccia clasts. No wall rock alteration. Handlens for scale. (b, c) Optical micrographs in plane polarized (b) and cross polarized (c) light showing plagioclase-rich wall rock clasts in a fine-grained former melt pocket. (d, e) Complex dark pseudotachylyte in paragneiss host. Note the finer grain size of the feldspar between the pseudotachylyte veins, indicating seismic fragmentation. Plane polarized (d) and cross polarized (e) light. (Sample HAM-1.)

to the pseudotachylytes, or between neighboring pseudotachylyte veins, the feldspar is heavily fractured (Figures 15d and 15e).

One pseudotachylyte-bearing fault juxtaposes rocks of different mineralogy (Figure 16a), one rich and one poor in pyroxene and amphibole, implying a displacement of at least 5 cm. The absence of wall rock alteration and shear in this locality shows that in the absence of fluids, seismic activity and pseudotachylyte formation did not trigger a significant metamorphic transformation of the metastable wall rocks, nor does it necessarily show a progression into the ductile deformation and shear zone development that is commonly observed in the Bergen Arcs. In this way, the Moskenesøya faults resemble the faulting observed in the Musgrave Block in Central Australia where pseudotachylytes are generated in completely dry lower crustal granulites without noticeable metamorphism. In the Musgrave case, however, voluminous pseudotachylyte formation may have weakened the crust, leading to mylonitization and interseismic creep even in the dry lithologies (Hawemann et al., 2018; Hawemann et al., 2019; Wex et al., 2017).

### 4.2. Mylonitized Pseudotachylytes at Nusfjord

On the eastern ridge of Nusfjord, amphibolite facies mylonitized and, to a lesser extent, pristine pseudotachylytes are found in three main sets of steeply dipping structures striking ENE-WSW to NE-SW (set 1), NW-SE (set 2), and NNE-SSW (set 3; Menegon et al., 2017). Mylonitized pseudotachylyte fault veins are identified by the local preservation of pseudotachylyte breccia pockets and injection veins (Figure 17a). Set 1 contains the largest volume of pseudotachylytes, but all sets do contain pseudotachylytes and share similar
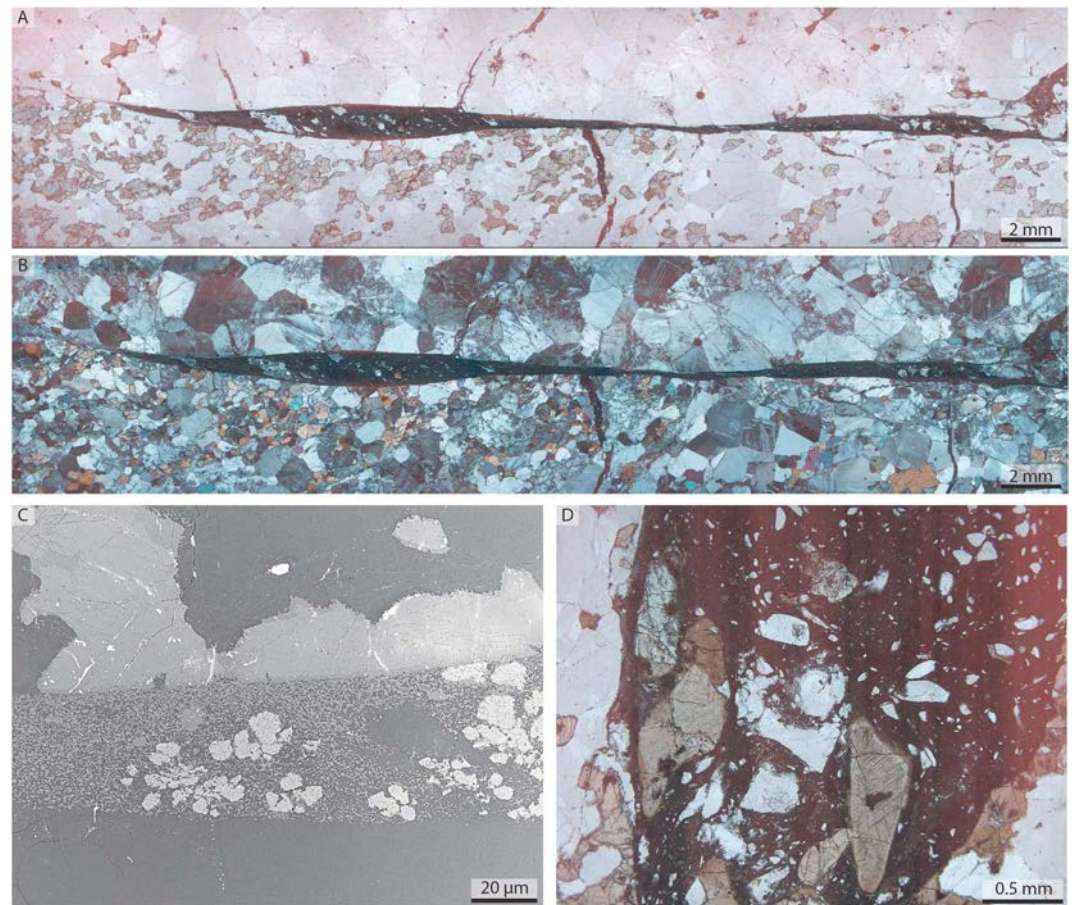
**Figure 16.** Pseudotachylyte in amphibole-bearing paragneiss. Optical micrographs in plane polarized (a) and cross polarized (b) light showing a pseudotachylyte that juxtaposes pyroxene and amphibole-rich (bottom) and poor (top) host rock. There is no alteration zone around the pseudotachylyte. (c) Backscatter electron image of the pseudotachylyte cutting pyroxene grains that exhibit alteration rims of amphibole. The pseudotachylyte contains a fine-grained mixture of plagioclase and pyroxene, some larger, slightly strained plagioclase clasts, and dendritic garnet with some euhedral overgrowths. (d) Optical micrograph (plane polarized light) of a pseudotachylyte containing numerous clasts of plagioclase (white), pyroxene (pale green), and amphibole (greenish brown). There is no evidence for amphibolitization of a preexisting eclogite-facies assemblage.

geometries. First-order mylonitic shear zones are up to 2- to 3-m wide and exploit the pseudotachylyte fault veins. The thickest shear zones may be derived from cyclical viscous overprint of several generations of pseudotachylytes, as indicated by the local occurrence of pseudotachylyte veins discordant to the main mylonitic foliation and only partially transposed into it. First-order shear zones are associated with subparallel second-order (centimeter-decameter thick) shear zones which also preferentially exploit pseudotachylyte veins. Individual shear zones show great lateral continuity, locally >1 km.

The best examples of pristine pseudotachylytes are found within lozenges of low strain domains of massive anorthosites bounded by first-order mylonitic shear zones that in turn exploited pseudotachylyte fault veins (Campbell et al., 2018). Pristine pseudotachylyte veins within the lozenges range in thickness from 0.7 to 18 mm, are 2- to 12-m long, and show coseismic displacements ranging from 1 to 26 cm, as constrained by the size of pull-apart openings between stepped veins (Figure 17b). Pseudotachylytes consist of single-generation individual fault veins with no evidence of multiple slip events along the same fault.

Pristine pseudotachylytes show chilled margins and flow structures, contain lithic clasts of plagioclase and clinopyroxene, and microlites of plagioclase ($An_{46-58}$), clinopyroxene (diopside), amphibole, and orthopyroxene in a microcrystalline (average grain size <5 μm) plagioclase-rich matrix (Figures 17c and 17d). Amphibole is absent from the anorthosite host rock, with the exception of rare amphibole-rich coronas
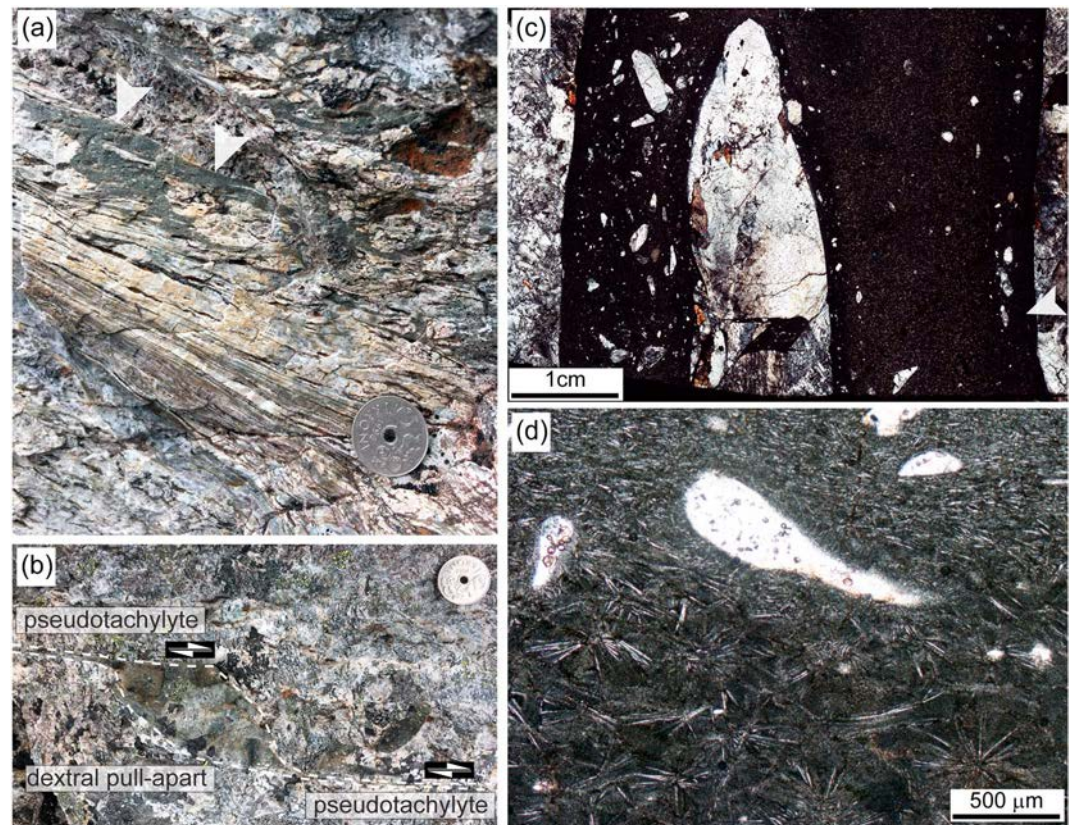
**Figure 17.** (a) Example of mylonized pseudotachylyte from Nusfjord. Weakly overprinted pseudotachylyte breccia is evident in the upper part of the image and is indicated by white triangles. (b) Example of dextral pull-apart between two pristine (nonmylonitized) pseudotachylyte veins. (c) Thin section of a pristine (nonmylonitized) pseudotachylyte sample hosted in undeformed anorthosite. Note the chilled margin at the pseudotachylyte vein boundaries (white arrow). Light microscope, crossed polarizer. (d) Microstructure of a pristine pseudotachylyte vein, showing microlites and lithic clasts of plagioclase. Alignment of microlites in the upper part of the image indicates primary flow structures in the frictional melt. Light microscope, crossed polarizer.

around magmatic clinopyroxene grains. Minor biotite is the only other hydrous mineral present in the anorthosite host rock (<1 vol%). The damage zone flanking pseudotachylyte veins contains fractured grains of plagioclase and clinopyroxene, filled by neoblasts of plagioclase and clinopyroxene $\pm$ amphibole, respectively (Figures 18a and 8b). There is no clear evidence of offset accommodated by the healed fractures (Figure 18b).

The mylonitized pseudotachylytes consist of a fine-grained (average grain size: 5–30 μm) mixture of plagioclase ($An_{46-58}$), amphibole (pargasite), and clinopyroxene (diopside), with minor amounts of garnet, biotite, quartz, and K-feldspar. There are no compositional changes in plagioclase, amphibole and clinopyroxene from the pristine to the mylonitized pseudotachylytes. In the mylonitized pseudotachylytes, clinopyroxene is partially to be completely replaced by fine-grained (<40 μm) aggregates of clinopyroxene + amphibole $\pm$ quartz that form highly elongated layers along the foliation (Figures 18c and 18d). These aggregates formed as a result of the following hydration reaction:

$$\text{Clinopyroxene} + \text{Plagioclase}_1 + H_2O = \text{Amphibole (Pargasite)} + \text{Plagioclase}_2 + \text{Quartz}$$
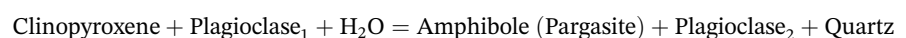
where the subscripts 1 and 2 refer to primary and recrystallized plagioclase, respectively. Such reaction has been observed also in other feldspar rich lower crustal shear zones in Lofoten, and indicates P-T conditions of 0.65–0.8 GPa, 700–730 °C (Menegon et al., 2013).

Amphibole forms 5–10 vol% of the mylonitized pseudotachylytes, and it typically occurs as isolated grains at triple junctions between plagioclase grains, in elongate trails parallel to C′ shear bands, and in the
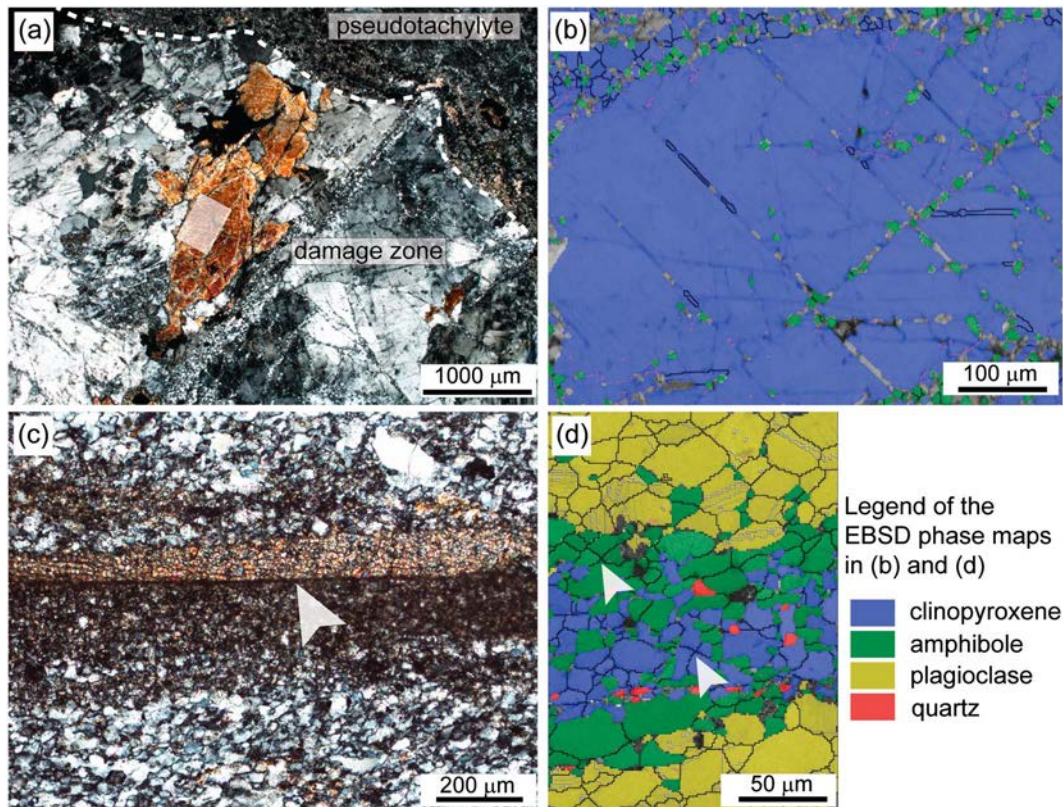
**Figure 18.** (a) Microstructure of clinopyroxene and plagioclase in the damage zone flanking a pristine pseudotachylyte vein, evident in the upper right side of the image. The white rectangle shows the location of the EBSD map shown in (b). Light microscope image, crossed polarizers. (b) EBSD phase map of the site indicated in (a). Black lines indicate high-angle boundaries (misorientation >10°), purple lines indicate low-angle boundaries (misorientation between 2° and 10°). (c) Microstructure of mylonitized pseudotachylyte. The image shows a compositional banding between plagioclase-dominated layers and clinopyroxene-derived layers, indicated by an arrowhead. Light microscope image, crossed polarizers. (d) EBSD phase map of a clinopyroxene-derived layer similar to the one shown in (c). Black lines indicate high-angle boundaries (misorientation >10°), purple lines indicate low-angle boundaries (misorientation between 2° and 10°), white lines indicate twin boundaries in plagioclase. White arrows indicate examples of quadruple junctions between grains. EBSD = electron backscatter diffraction.

clinopyroxene-derived layers. Amphibole and plagioclase do not show a crystallographic preferred orientation. Plagioclase and clinopyroxene grains in the damage zone flanking mylonitized pseudotachylytes contain fractures with no visible offset and filled with neoblasts of plagioclase and of clinopyroxene ± amphibole, respectively. These microstructures are identical to those in the damage zone around pristine pseudotachylyte veins.

### 4.3. Fluid Introduction and Transition to Shear Zones at Nusfjord

Field observations in Nusfjord indicate that mylonitic shear zones are genetically related to pseudotachylytes (Menegon et al., 2017; Steltenpohl et al., 2006), with the examples of Nusfjord East clearly demonstrating that mylonitic shear zones nucleated on pseudotachylyte fault veins. This indicates that pseudotachylyte veins were weaker than the surrounding host rock during viscous deformation.

The observations described above suggest that the infiltrated $H_2O$ was distributed at the grain and phase boundaries and promoted syn-kinematic phase nucleation during viscous shearing, as demonstrated by the occurrence of amphibole in triple junctions and C′ bands. The lack of CPO of amphibole and plagioclase, together with the high degree of phase mixing, the fine grain size of all phases, the frequent occurrence of quadruple grain junctions (Figure 18d), and the spatial distribution of amphibole, are consistent with diffusion creep, viscous grain boundary sliding and creep cavitation as the main deformation mechanisms in the mylonitized pseudotachylytes. Fluid-assisted, syn-kinematic nucleation of new phases inhibited grain growth and caused strain localization in the polymineralic, fine-grained mylonitied pseudotachylytes. Therefore, water introduction along grain boundaries had a major rheological effect on lower crustal shear zones, by facilitating diffusion creep deformation and phase nucleation.

**Figure 19.** Relatively weak mylonitized pseudotachylyte, as indicated by the moderate angle between the long axis of the stretched lithic clasts of anorthosite (white domains) and the shear zone (pseudotachylyte) boundary.

Extrapolation of laboratory derived flow laws for a temperature of 700 °C and strain rates in the range $10^{-10}$ to $10^{-14}$ s$^{-1}$ indicates a viscosity reduction of ~ 7 orders of magnitude during the formation of mylonitized pseudotachylytes deforming by diffusion creep compared to the dry anorthosite host (Menegon et al., 2017). Thus, pseudotachylyte veins provided the necessary weak, hydrated material capable of localizing viscous deformation in otherwise dry and strong granulites. This highlights the fundamental role of earthquakes as agents of rheological weakening in the dry lower crust through combined grain size reduction and fluid infiltration. It is worth noting that the fine grain size of the mylonitized pseudotachylytes at Nusfjord does not reflect a progressive strain dependent grain size reduction, as indicated by the occurrence of homogeneously fine-grained mylonitized veins at relatively low strain (Figure 19). This observation suggests that fine-grained, recrystallized pseudotachylytes were readily available as weak material capable to localize solid-state viscous deformation after the coseismic stage, and further highlights the fundamental role that earthquakes play in governing the short- and long-term rheological behavior of the lower crust through abrupt variations in material properties induced by seismic cycles.

### 4.4. Eclogites in Shear Zones at Flakstadøya

Eclogites or retrograded eclogites have been described from several localities at Flakstadøya in Lofoten (Froitzheim et al., 2016; Kullerud et al., 2001; Markl & Bucher, 1997; Steltenpohl et al., 2006). They invariably occur in shear zones embedded in feldspar-rich host rocks. Conditions of formation were initially estimated at 1.1–1.5 GPa pressure and a temperature of 650–700 °C (Kullerud et al., 2001; Markl & Bucher, 1997), but a recent study suggests pressures approaching 2.8 GPa (Froitzheim et al., 2016).

Interestingly, Steltenpohl et al. (2006) provided convincing evidence that eclogites and pseudotachylytes are cogenetic. The presence of an amphibolite facies mineralogy within the pseudotachylytes was thought to reflect retrogression of an original eclogite facies assemblage. Reexamination of pseudotachylytes from Moskenesøy do, however, provide undisputable microstructural evidence that the plagioclase-bearing amphibolite facies assemblage in the pseudotachylytes is primary (as is the case for pseudotachylytes from Nusfjord and other localities), and not a product of retrograde metamorphism of an eclogite facies assemblage (Figures 16c and 16d). Hence, like in the Bergen Arcs case, amphibolite- and eclogite-facies mineral assemblages appear to form synchronously, and the occurrence of eclogite is confined to rheologically weak shear zones. This is again consistent with high-P metamorphism due to weakening induced pressure perturbations at "normal" lower crustal depths and not to subduction to extreme depths (~90 km) as proposed by Froitzheim et al. (2016).

## 5. Laboratory Experiment Constraints

The lower crustal seismic faults described above have all formed at a confining pressure around 1 GPa, and the associated microstructures often show evidence of considerable recrystallization and recovery developed at low stress conditions. Hence, any submicrometer scale features or amorphous material that might have formed during high stress conditions would have been obliterated by such processes. To study the state of seismic faults at high confining pressure immediately after a slip event, it is necessary to conduct laboratory experiments. Incel et al. (2017) carried out such experiments on two lawsonite-bearing blueschists using the D-DIA apparatus mounted on the GSECARS 13 BM-D beamline at the Advanced Photon Source synchrotron, Argonne National Laboratory, Illinois, USA (Wang et al., 2003). The blueschists were deformed at a strain rate of approximately $10^{-5}$ s$^{-1}$ at confining pressures of 2.5–3 GPa. Based on recorded acoustic emissions and microstructural observations of the recovered samples, faulting was demonstrated to occur at a differential stress of ~3 GPa, in a temperature range of ~370–450 °C, and an axial strain of 5–19%. Seismic slip was interpreted to occur during the transition from lawsonite-blueschist to lawsonite-eclogite (Incel et al., 2017).
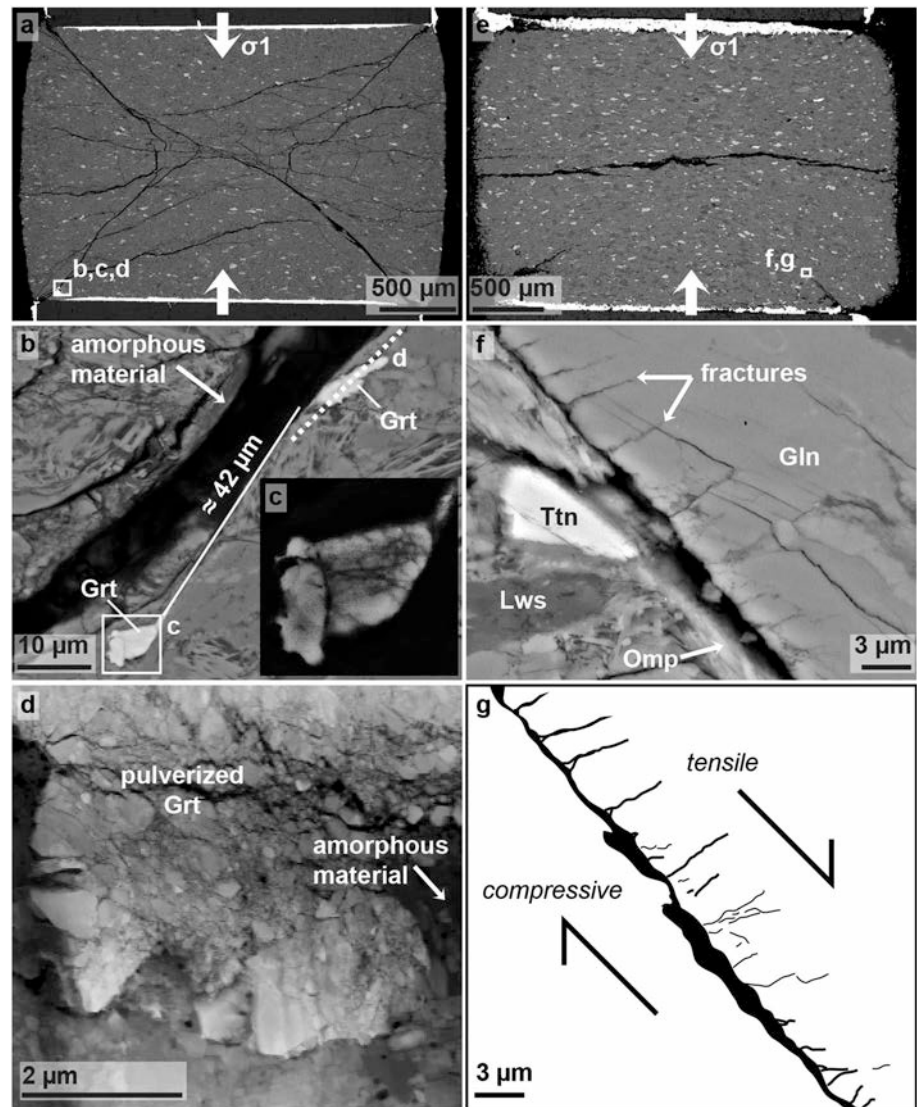
**Figure 20.** (a) BSE image of blueschist sample deformed at 3 GPa confining pressure in the temperature range 310–800 °C (Incel et al., 2017). The sample is cross cut by conjugated faults. (b) Example of fault that dissected and displaced a garnet crystal and is filled by amorphous material. The offset of the garnet fragments is ~42 μm. Dashed white line shows the location of a focused-ion beam section across garnet fragment shown in (d). (c) Extensively fractured garnet fragment (from lower left corner in (b) displaying micrometer and submicrometer-sized fragments. (d) Transmission electron microscope image of the focused-ion beam section in (b) reveals that the garnet is pulverized into micrometer- to nanometer-sized grains and also contain amorphous domains (from Incel, 2017). (e) Blueschist sample deformed at 2.5 GPa at a temperature range of 380–655 °C. Several fractures commence in the corners of the sample. (f) A set of parallel fractures can be observed on one side of the main fault. (g) Schematic drawing based on the backscattered image shown in (f). The shear sense along this fault is demonstrated with black arrows. The parallel tensile fractures are restricted to one side of the fault. Abbreviations not given in Figure 4: Gln = glaucophane; Ttn = titanite; Lws = lawsonite; BSE = backscattered electrons.

Under these conditions, faulting both causes the formation of amorphous material and fragmentation of fault wall rocks to nanometer-scale particles (Figures 20a–20d). Locally, faults display asymmetric wall rock damage with sets of parallel tensile fractures developed on one side of the slip plane. These structures resemble the feather features from the Bergen Arcs (Figure 6; Petley-Ragan et al., 2018). Such asymmetric effects are in agreement with theoretical studies of dynamic shear rupture which show that off-fault damage concentrates in the extensional side of the main fault (Poliakov et al., 2002; Rice et al., 2005). At high rupture velocities ($\geq 0.8\ c_s$) and high angles relative to the maximum compression direction (~45–60°), one side of
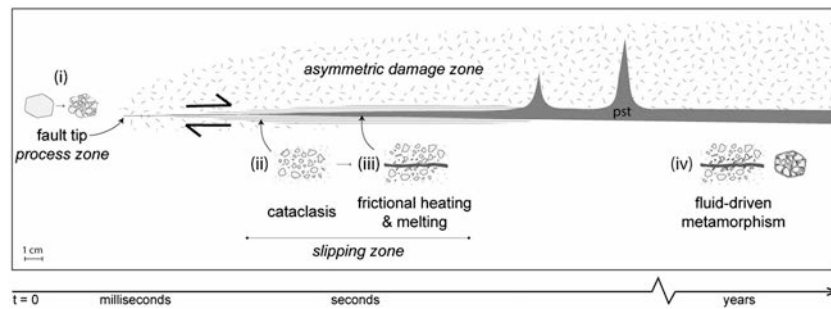
**Figure 21.** Temporal evolution of deformation processes in a seismic fault (from Petley-Ragan et al., 2019). The fault propagates from right to left and the time since the rupture tip passed increases to the right. Wall rock fragmentation occurs near the rupture tip (i). Dextral shear motion concentrates within the rupture zone behind the tip and the damaged rock undergoes cataclasis (ii). Accumulation of shear motion within the cataclasites leads to frictional heating and melting (iii). Melt products are injected into the damage zone and the cataclasites are completely molten where the volume of damaged wall rock is greatest. Metamorphism (green) creates growth rims around the clasts in the cataclasites and coronae around fragmented grains in the damage zone (iv).

the fault will experience tensile stress and will be prone to failure, because the tensile strength of rocks and minerals is far lower than the compressive strength.

In a fluid-present situation, asymmetric fracturing of wall rocks will also lead to an asymmetric progress of fluid-driven metamorphism and hence to a preferential weakening of the dilatant side of the dynamic ruptures. This would subsequently lead to preferential onset of ductile shear on one side of the fault plane as observed in Figure 9. Progressive ductile shear deformation will eventually obliterate this asymmetry to produce the familiar macroscopic structure of lower crustal shear zones (cf. Figure 11).

## 6. Dynamic Rupture and Damage in the Deep Crust

### 6.1. Damage Asymmetry

The observed asymmetric wall rock damage, along with microstructural observations suggesting very high stress levels near pseudotachylyte veins, are consistent with a fault evolution that includes a single seismic failure. A propagating dynamic shear rupture produced symmetric fracturing at the rupture tip (the process zone), asymmetric cracking, and fragmentation of the wall rock (the damage zone) and shear motion in the region behind the front (the slipping zone; Figure 21; Petley-Ragan et al., 2019). The asymmetric damage zone develops on the dilatant side of the fault (Griffith et al., 2012). During dynamic rupture, the main phase of wall rock damage occurs before frictional sliding causes melting and wall rock heating and is reflected by pseudotachylyte injection veins cutting into fragmented wall rocks (cf. Figure 4c). In this model, pulverization (fragmentation with negligible shear strain) of wall rock minerals most likely occurs due to a reduction of elastic moduli in the fractured regions. This produces damage-related radiation with a strong isotropic component (Ben-Zion & Ampuero, 2009) and provides a mechanism of wall rock pulverization that would be effective both in the upper and lower crust. A consistent fragment size area distribution with a power-law exponent of $-2$ ($-3$ for the corresponding radius distribution) for pulverized wall rocks from both shallow and deep earthquakes supports this model. Comminution of wall rock minerals by thermal shock during deep seated earthquakes as suggested by Papa et al. (2018) would not be expected to develop asymmetrically on only one side of a fault (Figures 4c and 9). High thermal stress levels would furthermore be confined to submillimeter distances from the slip surface.

### 6.2. Confinement Effects and Variation of Damage Zone Thickness With Depth

Field observations (Austrheim et al., 2017; Petley-Ragan et al., 2018; Rempe et al., 2013) and laboratory measurements (Incel, 2017; Yuan et al., 2011) demonstrate that the width of wall rock damage and pulverization (fragmentation with negligible strain) zones become increasingly narrow with increasing depth/pressure. This observation has also been confirmed by models showing the dependence of coseismic off-fault damage with depth (Okubo et al., 2019). Near the Earth's surface (e.g., across the San Andreas fault; Rempe et al., 2013) the damage zone may reach exceed 100 m, with a pulverization threshold at around 50 m from the
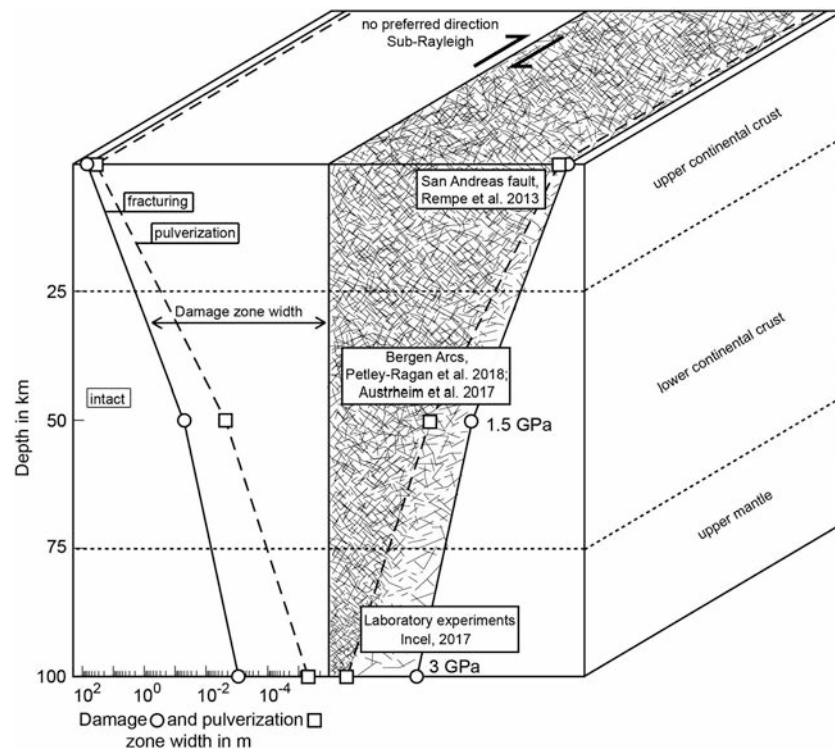
**Figure 22.** Schematic diagram showing the relation between depth/confining pressure and damage (black line and open circles) and pulverization (dashed black line and open squares) zone width based on field and laboratory observations. Systematic loading by sub-Rayleigh shear ruptures without preferred propagation direction would create a symmetrical damage zone across the fault in a homogeneous material (Aben et al., 2017).

fault core. These are however formed during repeated slip events. In the lower crust, at approximately 40- to 50-km depth and a pressure of 1.0–1.5 GPa, the width of the observed damage zone is on the order of 5 cm and pulverization is in a millimeter-wide zone across the fault (Austrheim et al., 2017; Petley-Ragan et al., 2018). Experimentally produced faulting accompanied by acoustic emissions performed at 3 GPa confining pressure resulted in wall rock pulverization of a millimeter-wide zone across the faults (Figure 20; Incel, 2017). Because of the small sample size (~2 mm) and because the sample also exhibits cross-cutting faults, the asymmetrical damage zone width could not be accurately measured, but is probably close to the length scale of the sample. Figure 22 shows how the zone of wall rock damage and pulverization gets narrower with increasing confinement, based on the observations described above.

Although the damage zone at lower crustal depth is rather narrow (1–10 cm), the intensity of fracturing is very high, and the permeability and reactive surface areas in the presence of fluids are correspondingly high (Mitchell & Faulkner, 2012). Weakening of fault wall rocks by metamorphic transformation processes will thus be effective, contributing to a swift transition toward ductile deformation and shear zone development.

## 7. Origin of Deep Crustal Earthquakes

The observations from the Norwegian Caledonides presented above, along with the ongoing seismic activity during the India-Tibet collision show that lower crustal earthquakes are common and may have large effects on the petrological and petrophysical evolution of "continental roots." They occur in dry and strong lithologies, and when associated with introduction of fluids they trigger metamorphic transformation processes and a pronounced local weakening. This effect, in turn, initiates ductile deformation and shear zone development which may affect a significant fraction of the lower crust, as observed in the Bergen Arcs.

Deep crustal earthquakes may, however, also occur in the absence of fluids. This is observed at Moskenesøya in Lofoten as described above, and has also been reported from the Musgrave ranges in Central Australia
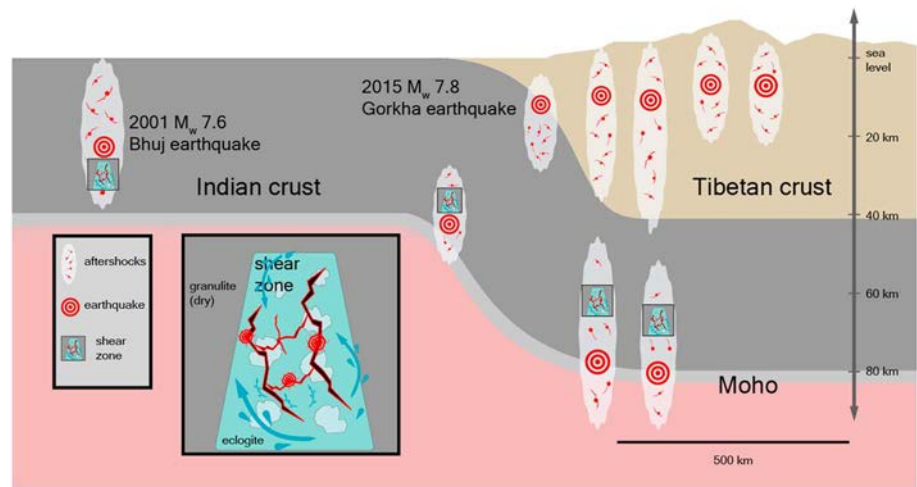
**Figure 23.** Schematic representation of earthquakes and aftershocks for the India-Tibet continent-continent collision. Each major earthquake generates a cloud of aftershocks, some of which are located in the lower crust (many aftershocks in the upper crust are not shown in this simple diagram). These aftershocks create pathways for fluids (blue arrows in insets), allowing partial hydration and metamorphism of the strong and dry granulites into wet and weaker eclogites and amphibolites. This process also facilitates the development of shear zones in the continental lower crust. For the subduction geometry, fluids could originate from the slab below or from the upper crust above. For the continental collision below the Himalayas, fluids introduced to the subducted Indian plate could originate from dehydration within the slab or from the dehydration of serpentine-containing mantle rocks below. Modified from Jamtveit, Ben-Zion, et al. (2018).

(Hawemann et al., 2018). Seismic slip by brittle failure in dry lower crust require stresses at a level that can only be sustained over short timescales or local weakening mechanisms. Local fluid production and weakening of rocks containing amphibole or other hydrous mineral has been proposed to explain the deep earthquakes in the lower parts of the subducted Indian crust (Hetényi et al., 2007). However, the granulites in the Bergen Arcs and Lofoten Archipelago are very dry and, at least at Moskenesøya in Lofoten, seismic slip occurred even in the absence of fluids. At both locations, there is no evidence for shear deformation prior to initial pseudotachylyte formation. A thermal runaway initiation of the earthquakes (Braeck & Podladchikov, 2007; Kelemen & Hirth, 2007) therefore seems unlikely. A transient increase in the stress state of the lower crust thus seems to be the most plausible alternative for the earthquake activity in the Bergen Arcs and in the Lofoten Archipelago.

Ellis and Stöckhert (2004) showed that regular earthquake activity in the seismogenic zone produces stress pulses in the lower crust. Such stress pulses may drive aftershocks to lower crustal levels as observed for example during the 2001 $M_W$ 7.6 Bhuj earthquake in India (Copley et al., 2011). Figure 23 shows a possible distribution of primary earthquakes and aftershocks in the India-Tibet case. Jamtveit, Ben-Zion, et al. (2018) showed that the volume of lower crust affected by aftershocks triggered by earthquakes in the normal seismogenic regime is very significant.

An interesting observation both from the Lofoten area and from the Musgrave ranges in Australia is an apparent interplay between ductile and brittle deformation. An initial stage of brittle failure and pseudotachylyte formation is followed by ductile shear and mylonite formation along the pre-existing pseudotachylytes. In many cases, however, a younger generation of pseudotachylytes develops within the mylonite bands, and this process may reiterate and produce several generations of brittle and ductile features superimposed on each other. Hawemann et al. (2019) proposed that this observation suggest a local (deep) source for the lower crustal earthquakes. An alternative model for systems located within the brittle-ductile transition zone was recently proposed by Aharonov and Scholz (2019). According to this model, mylonites in the brittle-ductile transition zone deform by low-temperature plasticity in a velocity-hardening regime under "normal" tectonic stress conditions. However, following a large earthquake in the shallower brittle regime and an associated stress and velocity increase within the brittle-ductile transition zone, the deeper system may be driven into a velocity-weakening regime and subsequently fail by frictional sliding. Stress reduction would then result in a transition to velocity-strengthening and a new generation of mylonite would form and

creep plastically until a new seismic event at shallow levels kick off another deep earthquake. For a dry feldspar-rich lower crust, it seems plausible that the brittle-ductile transition zone extends all the way to the bottom of the crust, and hence this mechanism may explain several superimposed generation of mylonites and pseudotachylytes both in Lofoten in in the Musgrave Range region.

## 8. Constraints on Lower Crustal Strength

In this paper we argue that the lower crust is strong *prior to* orogeny. This is mainly based on what we observe in the field both in the Bergen Arcs and the Lofoten areas. Figure 11 demonstrates that plagioclase-rich granulites are stronger than both eclogitized and amphibolitized rock volumes which develop into ductile shearzones while the granulites remain largely undeformed. We furthermore observe dynamic rupturing and subsequent seismic slip at lower crustal confining pressures (1–1.5 GPa). In the Lofoten case, this even occurs in completely dry rocks where no fluids were present to reduce the effective pressure (Figure 15). Abundant brittle deformation in the lower crust require differential stresses approaching the confining pressure (Kohlstedt et al., 1995) and hence a very strong rheology. This is fully consistent with deformation experiments carried out on plagioclase dominated systems under dry (fluid absent) conditions, including those of Tullis and Yund (1992) which were performed on intact natural rocks at 1.5 GPa confining pressure and temperatures in the range 600 to 800 °C and show peak differential stresses approaching the confining pressure (1–1.5 GPa). These conditions overlap those inferred from the Bergen Arcs and Lofoten, and were carried out on similar rock types.

It is known that natural plagioclase contains some hydrogen even at fluid absent conditions and that hydrogen will weaken nominally anhydrous phases (Johnson, 2006). However, Rybacki and Dresen (2000) conducted experiments on plagioclase containing 400-650 ppm H/Si under fluid absent ("dry") conditions and obtained rheological properties consistent both with the experiments of Tullis and Yund, and the viscosity for the lower Indian crust estimated by Copley, Avouac, Hollingsworth, and Leprince (2011). In this connection it is important to notice that prior to orogeny, the continental crust is likely to be characterized by a steady state geothermal gradient where the Moho temperature will typically be in the range 400–700 °C depending on crustal thickness and heat flow conditions (Mareschal & Jaupart, 2013). Most experimental works claiming that the lower crust is weak and that the jelly-sandwich model is an adequate description of lower crustal rheology (cf. Wang et al., 2012) are carried out at temperatures >800 °C and strain rates in the range $10^{-4}$ to $10^{-6}\,s^{-1}$. Rescaling the rheological properties obtained under such conditions to realistic crustal conditions requires reliable estimates of the activation energy of the creep process. Wang et al. (2012) report activation energies in the range 210–270 kJ/mol. However, Rybacki and Dresen's (2000) experiments conducted at fluid absent conditions suggest values around 650 kJ/mol. Assuming that the latter results are valid for dry (but still H-bearing) plagioclase-dominated systems, the values obtained by Wang et al. (2012) would lead to a serious underestimation of rock strength for dry lower crust. In fact, the activation energies reported by these authors indicate fluid present conditions, which is not likely to apply to lower crustal pressure and temperature conditions (Yardley & Valley, 1997).

Based on such evidence, we propose that the general lack of seismicity in most continental lower crusts (Scholz, 2002) is due to the lower crust being strong, not weak. The lower crust may however become locally weakened *during* an orogeny due to internal fluid production by the breakdown of hydrous phases during burial and heating, or by input of fluids to volumes where permeable pathways are developed that connect the lower crust to an external fluid source.

## 9. Conclusion and Future Challenges

Phase petrological considerations as well as observations from current and ancient continental collision zones indicate that the lower crust is strong and dry prior to an orogenic event.

During orogeny, fluid introduction to the lower crust is often associated with earthquakes. Microstructural records indicate that lower crustal earthquakes may develop by brittle failure and that significant wall rock damage and fragmentation occur during propagation of dynamic ruptures, prior to frictional slip and associated melting. The width of this damage zone decreases with confining pressure and is typically on a millimeter to centimeter length scale for lower crustal earthquakes.

If fluids are introduced, incipient metamorphism leads to grain size reduction and weakening of the wall rocks, which subsequently may develop into ductile shear zones. When weak rock volumes are confined within highly stressed rocks, they may develop pressures significantly higher than lithostatic.

Following an initial and local earthquake-induced weakening of the lower crust, frictional seismic slip and localized shear may evolve into cycles, where several generations of pseudotachylytes and mylonites are located within the same deformation zones. We speculate that the transitions from velocity-strengthening to velocity-weakening conditions are triggered by recurrent earthquakes in the shallower, brittle, regime.

Earthquake- and fluid-triggered metamorphism of the lower continental crust in collision zones cause a major strength reduction and, in the case of eclogitization, also a density increase of initially plagioclase-dominated lithologies. In contrast, during extension and hydration of oceanic lithosphere, similar processes affecting exposed mantle peridotites along slow and ultraslow spreading ridges cause weakening and a pronounced density decrease during serpentinization. In this respect fluid-induced metamorphism responds to the geodynamic boundary conditions according to whether volume needs to be compressed or inflated.

### 9.1. Future Challenges

A prevailing strong continental crust prior to collision is in stark contrast to the dominant lithospheric strengths profile used in most large-scale geodynamic models. Future research needs to test whether this scenario also applies to other orogens, and if so, what the consequences of a strong lower crust will be for the stress distribution, stress transfer, and strain partitioning in the continental lithosphere during collision.

Field-based studies of deformation zones in lower crustal rocks always represent post-mortem examination of lithological units after an orogeny. Abundant and spatially distributed high strain zones commonly reported in such studies (cf. Bürgmann & Dresen, 2008) clearly reflect ductile behavior of a relatively weak lower crust. However, in the case of the Scandinavian Caledonides this weakening occurs due to fluid mediated transformation processes *during* orogeny. Prior to orogeny, the lower crust is strong. From studies of incompletely transformed crustal volumes, we observe that the initial alteration processes are highly localized. To test the validity of the conclusions presented above for a given case study, it is essential to establish the mechanisms of strain localization from the initially dry lower crustal rocks. Brittle deformation in the absence of fluids, as described from the Musgrave Ranges by Hawemann et al. (2018) and from Lofoten (Figure 15 above) is diagnostic of a high stress environment in a strong lower crust. In systems subject to fluid infiltration, the situation is often less clear. Detailed examination of fault wall-rock damage may however provide important clues that may help deciphering whether localization is controlled by brittle fracturing (Petley-Ragan et al., 2019) or by self-localizing ductile mechanisms (Braeck & Podladchikov, 2007; Kelemen & Hirth, 2007).

Finally, metamorphism of the lower crust requires the presence of fluids. These may be internally produced during heating as proposed by Hetényi et al. (2007) during subduction of the Indian crust, or externally derived as in the Bergen Arcs. While it is known that internal fluid production may cause embrittlement (Raleigh & Paterson, 1965), it is less well understood how the influx of external fluids is coupled to the deformation. Are earthquakes in the lower crust producing the permeability required to allow fluid infiltration, and if so are the fluids entering from above or below? Alternatively, are overpressured fluids or even hydrous melts entering the dry lower crust by hydrofracturing? If so, do they trigger faulting of a highly stressed lower crust by lowering the effective stress or by local reaction-induced weakening and associated stress transfer to a decreasing fraction of strong rocks (cf. Scambelluri et al., 2017)?

## References

Aben, F., Doan, M.-L., Gratier, J.-P., & Renard, F. (2017). Coseismic damage generation and pulverization in fault zones: insights from dynamic Split Hopkinson Pressure Bar experiments. In "Fault Zone Properties and Processes during Dynamic Rupture", Editors M. Thomas, T. Mitchell, H. Bhat. *AGU Geophysical Monograph*, 227, 47–80.

Andersen, T. B., Corfu, F., Labrousse, L., & Osmundsen, P. T. (2012). Evidence for hyperextension along the pre-Caledonian margin of Baltica. *Journal of the Geological Society*, 169, 601–612.

Aharonov, E., & Scholz, C. H. (2019). The brittle-ductile transition predicted by a physics based friction law. *Journal of Geophysical Research: Solid Earth*, 124, 2721–2737. https://doi.org/10.1029/2018JB016878

Andersen, T., Austrheim, H., & Burke, E. A. J. (1991). Mineral-fluid-melt interactions in high-pressure shear zones in the Bergen Arcs nappe complex, Caledonides of W Norway: Implications for the fluid regime in Caledonian eclogite-facies metamorphism. *Lithos*, 27(3), 187–204. https://doi.org/10.1016/0024-4937(91)90012-A

Aupart, C., Dunkel, K. G., Angheluta, L., Austrheim, H., Ildefonse, B., Malthe-Sørenssen, A. M., & Jamtveit, B. (2018). Olivine grain size distributions in faults and shear zones: Evidence for non-steady state deformation. *Journal of Geophysical Research: Solid Earth*, *123*, 7421–7443. https://doi.org/10.1029/2018JB015836

Austrheim, H. (1987). Eclogitization of lower crustal granulites by fluid migration through shear zones. *Earth and Planetary Science Letters*, *81*(2-3), 221–232. https://doi.org/10.1016/0012-821X(87)90158-0

Austrheim, H. (2013). Fluid and deformation induced metamorphic processes around Moho beneath continent collision zones: Examples from the exposed root zone of the Caledonian mountain belt, W-Norway. *Tectonophysics*, *609*, 620–635. https://doi.org/10.1016/j.tecto.2013.03.030

Austrheim, H., & Boundy, T. M. (1994). Pseudotachylytes generated during seismic faulting and eclogitization of the deep crust. *Science*, *265*(5168), 82–83. https://doi.org/10.1126/science.265.5168.82

Austrheim, H., Dunkel, K. G., Plümper, O., Ildefonse, B., Liu, Y., & Jamtveit, B. (2017). Fragmentation of wall rock garnets during deep crustal earthquakes. *Science Advances*, *3*(2), e1602067. https://doi.org/10.1126/sciadv.1602067

Ben-Zion, Y., & Ampuero, J.-P. (2009). Seismic radiation from regions sustaining material damage. *Geophysical Journal International*, *178*(3), 1351–1356. https://doi.org/10.1111/j.1365-246X.2009.04285.x

Bhowany, K., Hand, M., Clark, K., Reddy, S., Peaorce, M. A., Tucker, N. M., & Morrisey, L. J. (2018). Phase equilibria modeling constraints on P-T conditions during fluid catalysed conversion of granulite to eclogite in the Bergen Arcs, Norway. *Journal of Metamorphic Geology*, *36*(3), 315–342. https://doi.org/10.1111/jmg.12294

Bingen, B., Austrheim, H., Whitehouse, M. J., & Davies, W. J. (2004). Trace element signature and U-Pb geochronology of eclogite-facies zircon, Bergen Arcs, Caledonides of W Norway. *Contributions to Mineralogy and Petrology*, *147*(6), 671–683. https://doi.org/10.1007/s00410-004-0585-z

Bingen, D. W. J., & Austrheim, H. (2001). Zircon U-Pb geochronology in the Bergen arc eclogites and their Proterozoic protoliths, and implications for the pre-Scandian evolution of the Caledonides in western Norway. *Geological Society of America Bulletin*, *113*(5), 640–649. https://doi.org/10.1130/0016-7606(2001)113<0640:ZUPGIT>2.0.CO;2

Bischoff, S. H., & Flesch, L. M. (2018). Normal faulting and viscous buckling in the Tibetan Plateau induced by weak lower crust. *Nature Communications*, *9*(1), 4952. https://doi.org/10.1038/s41467-018-07312-9

Braeck, S., & Podladchikov, Y. Y. (2007). Spontaneous thermal runaway as an ultimate failure mechanism. *Physical Review Letters*, *98*(9), 095504. https://doi.org/10.1103/PhysRevLett.98.095504

Burov, E. B. (2011). Rheology and strength of the lithosphere. *Marine and Petroleum Geology*, *28*(8), 1402–1443. https://doi.org/10.1016/j.marpetgeo.2011.05.008

Butler, J. P., Beaumont, C., & Jamieson, R. A. (2015). Paradigm lost: Buoyancy thwarted by the strength of the Western Gneiss Region (ultra) high-pressure terrane, Norway. *Lithosphere*, *7*(4), 379–407. https://doi.org/10.1130/L426.1

Campbell, L., Menegon, L., Fagereng, Å., Pennacchioni, G., & Mariani, E. (2018). Lower crustal seismicity as a signature of strain compatibility within localised shear zone networks. *Geophysical Research Abstracts*, *20*, EGU2018–EGU9054.

Chandrasekhar, D. V., Burgmann, R., Reddy, C. D., Sunil, P. S., & Schmidt, D. A. (2009). Weak mantle in NW India probed by geodetic measurements following the 2001 Bhuj earthquake. *Earth and Planetary Science Letters*, *280*(1-4), 229–235. https://doi.org/10.1016/j.epsl.2009.01.039

Chen, W. P., & Molnar, P. (1983). Focal depths of intracontinental and intraplate earthquakes and their implication for the thermal and mechanical properties of the lithosphere. *Journal of Geophysical Research*, *88*(B5), 4183–4214. https://doi.org/10.1029/JB088iB05p04183

Clark, M. K., & Royden, L. H. (2000). Topographic ooze: Building the eastern margin of Tibet by lower crustal flow. *Geology*, *28*, 703–706.

Clerc, A., Renard, F., Austrheim, H., & Jamtveit, B. (2018). Spatial and size distribution of garnet grown in a pseudotachylyte generated during intermediate-depth earthquake. *Tectonophysics*, *733*, 159–170. https://doi.org/10.1016/j.tecto.2018.02.014

Connolly, J. A. D. (1997). Devolatilization- generated fluid pressure and deformation-propagated fluid flow during prograde regional metamorphism. *Journal of Geophysical Research*, *102*(B8), 18,149–18,173. https://doi.org/10.1029/97JB00731

Connolly, J. A. D. (2010). Metamorphic devolatilization and fluid flow: Time and spatial scales. *Elements*, *6*(3), 165–172. https://doi.org/10.2113/gselements.6.3.165

Connolly, J. A. D., & Podladchikov, Y. Y. (1998). Compaction-driven fluid flow in viscoelastic rock. *Geodinamica Acta*, *11*(2-3), 55–84. https://doi.org/10.1080/09853111.1998.11105311

Copley, A., Avouac, J.-P., Hollingsworth, J., & Leprince, S. (2011). The 2001 $M_W$ 7.6 Bhuj earthquake, low fault friction and the upper crustal support of plate driving forces in India. *Journal of Geophysical Research*, *116*, B08405. https://doi.org/10.1029/2010JB008137

Copley, A., Avouac, J.-P., & Royer, J.-Y. (2011). India-Asia collision and the Cenozoic slowdown of the Indian plate: Implications for the forces driving plate motions. *Journal of Geophysical Research*, *115*, B03410.

Corfu, F. (2004a). U–Pb age, setting and tectonic significance of the anorthosite–mangerite–charnockite–granite suite, Lofoten–Vesterålen, Norway. *Journal of Petrology*, *45*(9), 1799–1819. https://doi.org/10.1093/petrology/egh034

Corfu, F. (2004b). U-Pb geochronology of the Leknes Group: An exotic Early Caledonian metasedimentary assemblage stranded on Lofoten basement, northern Norway. *Journal of the Geological Society of London*, *161*(4), 619–627. https://doi.org/10.1144/0016-764903-066

Craig, T. J., Copley, A., & Jackson, J. (2012). Thermal and tectonic consequences of India underthrusting Tibet. *Earth and Planetary Science Letters*, *353-354*, 231–239. https://doi.org/10.1016/j.epsl.2012.07.010

Di Toro, G., Nielsen, S., & Pennacchioni, G. (2005). Earthquake rupture dynamics in exhumed ancient faults. *Nature*, *436*(7053), 1009–1012. https://doi.org/10.1038/nature03910

Ellis, S., & Stöckhert, B. (2004). Elevated stresses and creep rates beneath the brittle-ductile transition caused by seismic faulting in the upper crust. *Journal of Geophysical Research*, *109*, B05407.

Ellsworth, W. L. (2005). Injection-induced earthquakes. *Science*, *341*(6142), 1225942.

Froitzheim, N., Milandinova, I., Janak, M., Kullerud, K., Ravna, E. K., Majka, J., et al. (2016). Devonian subduction and syncollisional exhumation of continental crust in Lofotem, Norway. *Geology*, *44*(3), 223–226. https://doi.org/10.1130/G37545.1

Glodny, J., Kühn, A., & Austrheim, H. (2002). Rb/Sr record of fluid–rock interaction in eclogites, Bergen Arcs, Norway. *Geochimica et Cosmochimica Acta*, *66*(S1), A280.

Glodny, J., Kühn, A., & Austrheim, H. (2008). Geochronology of fluid-induced eclogite and amphibolite facies metamorphic reactions in a subduction-collision system, Bergen Arcs, Norway. *Contributions to Mineralogy and Petrology*, *156*(1), 27–48. https://doi.org/10.1007/s00410-007-0272-y

Griffith, W. A., Mitchell, T. M., Renner, J., & Di Toro, G. (2012). Coseismic damage and softening of fault rocks at seismogenic depths. *Earth and Planetary Science Letters*, *353*, 291–230.

Hacker, B. R., Andersen, T. B., Johnston, S., Kylander-Clark, A. R. C., Peterman, E., Walsh, E. O., & Young, D. (2010). High-temperature deformation during continental margin subduction and exhumation: The ultrahigh-pressure Western Gneiss Region of Norway. *Tectonophysics*, *480*(1-4), 149–171. https://doi.org/10.1016/j.tecto.2009.08.012

Hawemann, F., Mancktelow, N. S., Pennacchioni, G., Wex, S., & Camacho, A. (2019). Weak and slow, strong and fast: How shear zones evolve in a dry continental crust (Musgrave Ranges, Central Australia). *Journal of Geophysical Research: Solid Earth*, *124*, 219–240.

Hawemann, F., Mancktelow, N. S., Wex, S., Camacho, A., & Pennacchioni, G. (2018). Pseudotachylyte as field evidence for lower crustal earthquakes during the intracontinental Petermann Orogeny (Musgrave Block, Central Australia). *Solid Earth*, *9*(3), 629–648. https://doi.org/10.5194/se-9-629-2018

Hetényi, G., Cattin, R., Brunet, F., Bollinger, L., Vergne, J., Nabelek, J. L., & Diament, M. (2007). Density distribution of the India plate beneath the Tibetan plateau: Geophysical and petrological constraints on the kinetics of lower-crustal eclogites. *Earth and Planetary Science Letters*, *264*(1-2), 226–244. https://doi.org/10.1016/j.epsl.2007.09.036

Incel, S. (2017). Experimental constraints on rheology during eclogite-facies metamorphic reactions. PhD thesis, EarthSciences. PSL Research University, Paris. 209 p.

Incel, S., Hilairet, N., Labrousse, L., John, T., Deldicque, D., Ferrand, T. H., et al. (2017). Laboratory earthquakes triggered during eclogitizaiton of lawsonite-bearing blueschist. *Earth and Planetary Science Letters*, *459*, 320–331. https://doi.org/10.1016/j.epsl.2016.11.047

Jakob, J., Alsaif, M., Corfu, F., & Andersen, T. B. (2017). Age and origin of thin discontinuous gneiss sheets in the distal domain of the magma-poor hyperextended pre-Caledonian margin of Baltica, Southern Norway. *Journal of the Geological Society of London*, *174*, 541–571.

Jamtveit, B., Austrheim, H., & Malthe-Sørensen, A. (2000). Accelerated hydration of the Earth's deep crust induced by stress perturbations. *Nature*, *408*(6808), 75–78. https://doi.org/10.1038/35040537

Jamtveit, B., Austrheim, H., & Putnis, A. (2016). Disequilibrium metamorphism of stressed lithosphere. *Earth Science Reviews*, *154*, 1–13. https://doi.org/10.1016/j.earscirev.2015.12.002

Jamtveit, B., Ben-Zion, Y., Renard, F., & Austrheim, H. (2018). Earthquake-induced transformation of the lower crust. *Nature*, *556*, 487491.

Jamtveit, B., Moulas, E., Andersen, T. B., Austrheim, H., Corfu, F., Petley-Ragan, A., & Schmalholz, S. M. (2018). High pressure metamorphism caused by fluid induced weakening of deep continental crust. *Scientific Reports*, *8*(1), 17011. https://doi.org/10.1038/s41598-018-35200-1

Jamtveit, B., & Yardley, B. W. D. (1997). *Fluid flow and transport in rocks: Mechanisms and effects* (p. 319). London: Chapman and Hall. https://doi.org/10.1007/978-94-009-1533-6_1

Johnson, E. A. (2006). Water in nominally anhydrous crustal minerals: Speciation, concentration, and geological significance. *Reviews in Mineralogy and Geochemistry*, *62*(1), 117–154. https://doi.org/10.2138/rmg.2006.62.6

Kelemen, P. B., & Hirth, G. (2007). A periodic shear-heating mechanism for intermediate depth earthquakes in the mantle. *Nature*, *446*(7137), 787–790. https://doi.org/10.1038/nature05717

Kohlstedt, D. L., Evans, B., & Mackwell, S. J. (1995). Strength of the lithosphere—Constraints imposed by laboratory experiments. *Journal of Geophysical Research*, *100*, 17,587–17,602.

Koziol, A. M., & Newton, R. C. (1988). Redetermination of the anorthite breakdown reaction and improvement of the plagioclase-garnet-$Al_2SiO_5$-quartz geobarometer. *American Mineralogist*, *73*, 216–223.

Kühn, A. (2002). The influence of fluid on the granulite to eclogite and amphibolite facies transition: a study in the anorthositic rocks from the Lindås Nappe, Bergen Arcs, West Norway. PhD Thesis, University of Oslo.

Kullerud, K., Flaat, K., & Davidsen, B. (2001). High-pressure fluid–rock reactions involving Cl-bearing fluids in lower-crustal ductile shear zones of the Flakstadøy basic complex, Lofoten, Norway. *Journal of Petrology*, *42*(7), 1349–1372. https://doi.org/10.1093/petrology/42.7.1349

Leib, S. E., Moecher, D. P., Steltenpohl, M. G., & Andresen, A. (2016). Thermobarometry of metamorphosed pseudotachylyte and associated mylonite: Constraints on dynamic co-seismic rupture depth attending Caledonian extension, North Norway. *Tectonophysics*, *682*, 85–95. https://doi.org/10.1016/j.tecto.2016.05.042

Mainprice, D., Backmann, F., Hielscher, R., & Schaeben, H. (2015). Descriptive tools for the analysis of texture projects with large datasets using MTEX: Strength, symmetry and components. *Geological Society, London, Special Publications*, *409*(1), 251–271. https://doi.org/10.1144/SP409.8

Mancktelow, N. S. (1993). Tectonic overpressure in competent mafic layers and the development of isolated eclogites. *Journal of metamorphic Geology*, *11*, 801–812

Mancktelow, N. S. (2006). How ductile are ductile shear zones? *Geology*, *34*, 345–348.

Mancktelow, N. S. (2008). Tectonic pressure: Theoretical concepts and modelled examples. *Lithos*, *103*, 149–177.

Mareschal, J.-P., & Jaupart, C. (2013). Radiogenic heat production, thermal regime and evolution of continental crust. *Teconophysics*, *609*, 524–534. https://doi.org/10.1016/j.tecto.2012.12.001

Markl, G., & Bucher, K. (1997). Proterozoic eclogites from the Lofoten islands, northern Norway. *Lithos*, *42*(1-2), 15–35. https://doi.org/10.1016/S0024-4937(97)00034-0

Markl, G., Frost, B. R., & Bucher, K. (1998). The origin of anorthosites and related rocks from the Lofoten Islands, Northern Norway: I. Field relations and estimation of intrinsic variables. *Journal of Petrology*, *39*(8), 1425–1452.

Menegon, L., Pennachioni, G., Malaspina, N., Harris, K., & Wood, E. (2017). Earthquakes as precursors of ductile shear zones in the dry and strong lower crust. *Geochemistry, Geophysics, Geosystems*, *18*, 4356–4374. https://doi.org/10.1002/2017GC007189

Menegon, L., Stünitz, H., Nasipuri, P., Heilbronner, R., & Svahnberg, H. (2013). Transition from fracturing to viscous flow in granulite facies perthitic feldspar (Lofoten, Norway). *Journal of Structural Geology*, *48*, 95–112. https://doi.org/10.1016/j.jsg.2012.12.004

Miller, S. A., Collettine, C., & Chiaraluce, L. (2004). Aftershocks driven by a high-pressure $CO_2$ source at depth. *Nature*, *427*(6976), 724–727. https://doi.org/10.1038/nature02251

Mitchell, T., & Faulkner, D. R. (2012). Towards quantifying the matrix permeability of fault damage zones in low porosity rocks. *Earth and Planetary Science Letters*, *339*, 24–31.

Mitchell, T. M., Ben-Zion, Y., & Shimamoto, T. (2011). Pulverized fault rocks and damage asymmetry along the Arima-Takatsuki tectonic line, Japan. *Earth and Planetary Science Letters*, *308*(3-4), 284–297. https://doi.org/10.1016/j.epsl.2011.04.023

Moecher, D. P., & Steltenpohl, M. G. (2009). Direct calculation of rupture depth for an exhumed paleoseismogenic fault from mylonitic pseudotachylyte. *Geology*, *37*(11), 999–1002. https://doi.org/10.1130/G30166A.1

Moecher, D. P., & Steltenpohl, M. G. (2011). Petrologic evidence for co-seismic slip in extending middle to lower continental crust: Heier's Zone of Pseudotachylyte, North Norway. In A. Fagereng, V. G. Toy, & J. V. Rowland (Eds.), *Geology of the earthquake source: A volume in honour of Rick Sibson, Geological Society of London, Special Publications* (Vol. 359, pp. 169–186). London: Geological Society of London. https://doi.org/10.1144/SP359.10

Monsalve, G., Sheehan, A., Schulte-Pelkum, V., Rajaure, S., Pandey, M. R., & Wu, F. (2006). Seismicity and one-dimensional velocity structure of the Himalayan collision zone: Earthquakes in the crust and upper mantle. *Journal of Geophysical Research*, *111*, B10301. https://doi.org/10.1029/2005JB004062

Moore, J., Beinlich, A., Austrheim, H., & Putnis, A. (2019). Stress-orientation dependent reactions during metamorphism. *Geology*, *47*, 151–154. https://doi.org/10.1130/G45632.1

Moulas, E., Burg, J. P., & Podladchikov, Y. (2014). Stress field associated with elliptical inclusions in a deforming matrix: Mathematical model and implications for tectonic overpressure in the lithosphere. *Tectonophysics*, *631*, 37–49. https://doi.org/10.1016/j.tecto.2014.05.004

Mukai, H., Austrheim, H., Putnis, C. V., & Putnis, A. (2014). Tectural evolution of plagioclase feldspar across a shear zone: Implications for deformation mechanisms and rock strength. *Journal of Petrology*, *55*(8), 1457–1477. https://doi.org/10.1093/petrology/egu030

Muto, J., Nakatani, T., Nishikawa, O., & Nagahama, H. (2015). Fractal particle size distribution of pulverized fault rocks as a function of distance from the fault core. *Geophysical Reseach Letteters*, *42*, 3811–3819. https://doi.org/10.1002/2015GL064026

Nakao, A., Iwamori, H., & Nakakuki, T. (2016). Effects of water transportation on subduction dynamics: Roles of viscosity and density reduction. *Earth and Planetary Science Letters*, *454*, 178–191. https://doi.org/10.1016/j.epsl.2016.08.016

Okubo, K., Bhat, H. S., Rougier, E., Marty, S., Schubnel, A., Lei, Z., et al. (2019). Dynamics, radiation and overall energy budget of earthquake rupture with coseismic off-fault damage. *Journal of Geophysical Research: Solid Earth*, *124*. https://doi.org/10.1029/2019JB017304

Papa, S., Pennacchioni, G., Angel, R. J., & Faccenda, M. (2018). The fate of garnet during (deep-seated) coseismic frictional heating: The role of thermal shock. *Geology*, *46*(5), 471–474. https://doi.org/10.1130/G40077.1

Petley-Ragan, A., Ben-Zion, Y., Austrheim, H., Ildefonse, B., Renard, F., & Jamtveit, B. (2019). Dynamic earthquake rupture in the lower crust. *Science Advances*, *5*. https://doi.org/10.1126/sciadv.aaw0913

Petley-Ragan, A., Dunkel, K. G., Austrheim, H., Ildefonse, B., & Jamtveit, B. (2018). Microstructural records of intermediate-depth earthquakes and associate fluid-driven metamorphism of plagioclase-rich granulites. *Journal of Geophysical Research: Solid Earth*, *123*, 3729-3746.

Plattner, U., Markl, G., & Sherlock, S. (2003). Chemical heterogeneities of Caledonian (?) pseudotachylites in the Eidsfjord Anorthosite, North Norway. *Contributions to Mineralogy and Petrology*, *145*(3), 316–338. https://doi.org/10.1007/s00410-003-0455-0

Plümper, O., John, T., Podladchikov, Y. Y., Vrijmoed, J., & Scambelluri, M. (2017). Fluid escape from subduction zones controlled by channel-forming reactive porosity. *Nature Geoscience*, *10*(2), 150–156. https://doi.org/10.1038/ngeo2865

Poelchau, M. H., & Kenkmann, T. (2011). Feather features: A low-shock-pressure indicator in quartz. *Journal of Geophysical Research*, *116*, B02201.

Poliakov, A. N. B., Dmowska, R., & Rice, J. R. (2002). Dynamic shear rupture interactions with fault bends and off-axis secondary faulting. *Journal of Geophysical Research*, *107*(B11), ESE 6-1–ESE 6-18. https://doi.org/10.1029/2001JB000572

Pristley, K., Jackson, J., & McKenzie, D. (2008). Lithospheric structure and deep earthquakes beneath Inida, the Himalaya and southern Tibet. *Geophysical Journal International*, *172*(1), 345–362. https://doi.org/10.1111/j.1365-246X.2007.03636.x

Putnis, A., Jamtveit, B., & Austrheim, H. (2017). Metamorphic processes and seismicity: the Bergen Arcs as a natural laboratory. *Journal of Petrology*, *58*(10), 1871–1898. https://doi.org/10.1093/petrology/egx076

Raleigh, C., & Paterson, M. (1965). Experimental deformation of serpentinite and its tectonic implications. *Journal of Geophysical Research*, *70*(16), 3965–3985. https://doi.org/10.1029/JZ070i016p03965

Rempe, M., Mitchell, T., Renner, J., Nippress, S., Ben-Zion, Y., & Rockwell, T. (2013). Damage and seismic velocity structure of pulverized rocks near the San Andreas Fault. *Journal of Geophysical Research: Solid Earth*, *118*, 2813–2831.

Rice, J. R., Sammis, C. G., & Parsons, R. (2005). Off-fault secondary failure induced by a dynamic slip pulse. *Bulletin of the Seismological Society of America*, *95*(1), 109–134. https://doi.org/10.1785/0120030166

Rockwell, T., Sisk, M., Girty, G., Dor, O., Wechsler, N., & Ben-Zion, Y. (2009). Chemical and physical characteristics of pulverized Tejon Lookout granite adjacent to the San Andreas and Garlock faults: Implications for earthquake physics. *Pure and Applied Geophysics*, *166*(10-11), 1725–1746. https://doi.org/10.1007/s00024-009-0514-1

Rybacki, E., & Dresen, G. (2000). Dislocation and diffusion creep of synthetic anorthite aggregates. *Journal of Geophysical Research*, *105*(B11), 26,017–26,036. https://doi.org/10.1029/2000JB900223

Rybacki, E., & Dresen, G. (2004). Deformation mechanism maps for feldspar rocks. *Tectonophysics*, *382*(3-4), 173–187. https://doi.org/10.1016/j.tecto.2004.01.006

Scambelluri, M., Pennacchioni, G., Gilio, M., Bestmann, M., Plümper, O., & Nestola, F. (2017). Fossil intermediate-depth earthquakes in subducting slabs linked to differential stress release. *Nature Geoscience*, *10*(12), 960–966. https://doi.org/10.1038/s41561-017-0010-7

Scholz, C. H. (2002). *The mechanics of earthquakes and faulting* (2nd ed., p. 471). New York: Cambridge University Press. https://doi.org/10.1017/CBO9780511818516

Schulte-Pelkum, V., Monsalve, G., Sheehan, A. F., Shearer, P., Wu, F., & Rajaure, S. (2019). Mantle earthquakes in the Himalaya collision zone. *Geology*. https://doi.org/10.1130/G46378.1

Shi, D., Zhao, W., Klemperer, S. L., Wu, Z., Mechie, J., Shi, J., et al. (2016). West-east transition from underplating to steep subduction in the India-Tibet collision zone revealed by receiver-function profiles. *Earth and Planetary Science Letters*, *452*, 171–177. https://doi.org/10.1016/j.epsl.2016.07.051

Shi, F., Wang, Y. B., Yu, T., Zhu, L. P., Zhang, J. F., Wen, J. G., et al. (2018). Lower-crustal earthquakes in southern Tibet are linked to eclogitization of dry metastable granulite. *Nature Communications*, *9*(1), 3483. https://doi.org/10.1038/s41467-018-05964-1

Sibson, R. H. (1996). Strutural permeability of fluid-driven fault-fracture meshes. *Journal of Structural Geology*, *18*(8), 1031–1042. https://doi.org/10.1016/0191-8141(96)00032-6

Sloan, R. A., Jackson, J. A., McKenzie, D., & Pristley, K. (2011). Earthquake depth distributions in central Asia, and their relations with lithosphere thickness, shortening and extension. *Geophysical Journal International*, *185*(1), 1–29. https://doi.org/10.1111/j.1365-246X.2010.04882.x

Steltenpohl, M. G., Hames, W. E., & Andresen, A. (2004). The Silurian to Permian history of a metamorphic core complex in Lofoten, northern Scandinavian Caledonides. *Tectonics*, *23*, TC1002. https://doi.org/10.1029/2003TC001522

Steltenpohl, M. G., Kassos, G., & Andresen, A. (2006). Retrograded eclogite-facies pseudotachylytes as deep-crustal paleoseismic faults within continental basement of Lofoten, north Norway. *Geosphere*, *2*(1), 61–72. https://doi.org/10.1130/GES00035.1

Steltenpohl, M. G., Moecher, D. P., Andresen, A., Ball, J., & Mager, S. (2011). The Eidsfjord shear zone: an Early Devonian, paleoseismogenic low-angle normal fault exposed in Lofoten-Vesterålen, north Norway. *Journal of Structural Geology*, *33*(5), 1023–1043. https://doi.org/10.1016/j.jsg.2011.01.017

Svensen, H., Jamtveit, B., Yardley, B. W. D., Engvik, A. K., & Austrheim, H. (1999). Lead and Bromine enrichment in eclogite facies fluids: Extreme fractionation during lower crustal hydration. *Geology*, *27*(5), 467–470. https://doi.org/10.1130/0091-7613(1999)027<0467: LABEIE>2.3.CO;2

Tullis, J., & Yund, R. (1992). The brittle-ductile transition in feldspar aggregates: An experimental study. *International geophysics*, *51*, 89–117.

VanWyck, N., Valley, J. W., & Austrheim, H. (1996). Oxygen and carbon isotope constraints on the development of eclogites, Holsnøy, Norway. *Lithos*, *38*(3-4), 129–145. https://doi.org/10.1016/0024-4937(96)00004-7

Von Blanckenburg, F. & Davies, J.H. (1995). Slab breakoff—A model for syncollisional magmatism in the Alps. *Tectonics*, *14*, 120-131, 1. https://doi.org/10.1029/94TC02051.

Walther, J. V., & Orville, P. M. (1982). Volatile production and transport in regional metamorphism. *Contributions to Mineralogy and Petrology*, *79*(3), 252–257. https://doi.org/10.1007/BF00371516

Wang, Y., Durham, W. B., Getting, I. C., & Weidner, D. J. (2003). The deformation-DIA: A new apparantus for high temperature triaxial deformation to pressures up to 15 GPa. *Review of Scientific Instruments*, *74*, 3301–3011.

Wang, Y. F., Zhang, J. F., Jin, Z. M., & Green, H. W. (2012). Mafic granulite rheology: Implications for a weak continental lower crust. *Earth and Planetary Science Letters*, *353-354*, 99–107. https://doi.org/10.1016/j.epsl.2012.08.004

Wechsler, N., Allen, E. E., Rockwell, T. K., Girty, G., Chester, J. S., & Ben-Zion, Y. (2011). Characterization of pulverized granitoids in a shallow core along the San Andreas Fault, Littlerock, CA. *Geophysical Journal International*, *186*(2), 401–417. https://doi.org/10.1111/j.1365-246X.2011.05059.x

Wex, S., Mancktelow, N. S., Hawemann, F., Camacho, A., & Pennacchioni, G. (2017). Geometry of a large-scale, low-angle, midcrustal thrust (Woodroffe Thrust, central Australia). *Tectonics*, *36*, 2447–2476. https://doi.org/10.1002/2017TC004681

Yardley, B. W. D. (1995). The evolution of fluids though the metamorphic cycle. In B. Jamtveit & B. W. D. Yardley (Eds.), *Fluid flow and transport in rocks: Mechanisms and effects* (pp. 99–121). London: Chapman and Hall.

Yardley, B. W. D., & Valley, J. W. (1997). The petrologic case for a dry lower crust. *Journal of Geophysical Research*, *102*(B6), 12,173–12,185. https://doi.org/10.1029/97JB00508

Yuan, F., Prakash, V., & Tullis, T. (2011). Origin of pulverized rocks during earthquake fault rupture. *Journal of Geophysical Research*, *116*, 1–18.

Zoback, M. D., & Townend, J. (2001). Implications of hydrostatic pore pressures and high crustal strength for the deformation of intraplate lithosphere. *Tectonophysics*, *336*(1-4), 19–30. https://doi.org/10.1016/S0040-1951(01)00091-9

## References From the Supporting Information

Jaffey, A. H., Flynn, K. F., Glendenin, L. E., Bentley, W. C., & Essling, A. M. (1971). Precision measurement of half-lives and specific activities of $^{235}$U and $^{238}$U. *Physical Review, Section C, Nuclear Physics*, *4*(5), 1889–1906. https://doi.org/10.1103/PhysRevC.4.1889

Krogh, T. E. (1973). A low contamination method for hydrothermal decomposition of zircon and extraction of U and Pb for isotopic age determinations. *Geochimica et Cosmochimica Acta*, *37*, 485–494.

Ludwig, K. R. (2009). *Isoplot 4.1. A geochronological toolkit for Microsoft Excel* (Vol. 4, p. 76). Berkeley Geochronology Center Special Publication.

Mattinson, J. M. (2005). Zircon U-Pb chemical abrasion ("CA-TIMS") method: combined annealing and multi-step partial dissolution analysis for improved precision and accuracy of zircon ages. *Chemical Geology*, *220*(1-2), 47–66. https://doi.org/10.1016/j.chemgeo.2005.03.011

Parrish, R. R., & Noble, S. R. (2003). Zircon U-Th-Pb geochronology by isotope dilution-thermal ionization mass spectrometry (ID-TIMS). In: J.M. Hanchar & P.W.O. Hoskin (Eds.), Zircon. *Reviews in Mineralogy and Geochemistry*, *53*, 183–213.

Stacey, J. S., & Kramers, J. D. (1975). Approximation of terrestrial lead isotope evolution by a two-stage model. *Earth and Planetary Science Letters*, *34*, 207–226.